RESEARCH ARTICLE

Using high-resolution Pb isotopes to unravel the petrogenesis of Sakurajima volcano, Japan

Joshua R. Brown[1] · Rex N. Taylor[1] · Masato Iguchi[2]

Abstract
Sakurajima volcano on the rim of Aira caldera erupts daily, threatening the major nearby population centre of Kagoshima. Before 1955, eruptions have typically consisted of intermittent Plinian and effusive activity, but since 1955, frequent Vulcanian explosions have occurred, indicating a change in pre-eruptive processes. High-resolution Pb isotopes are used here to constrain the components, including crustal assimilants, and petrogenetic processes contributing to the composition of both pre and post 1955 magmas. Sakurajima eruptive products have more radiogenic Pb ($^{206}Pb/^{204}Pb = 18.40–18.42$) than nearby Sumiyoshiike basalts ($^{206}Pb/^{204}Pb = 18.24$), a proxy for the primitive magma feeding the Sakurajima-Aira system. Sakurajima samples lie along a mixing line between these basalts and locally exposed crustal compositions. Their Pb isotopes are consistent with addition of ~ 5% average crustal melt to the primitive basaltic magma. The narrow range of Pb isotope ratios, despite variable SiO_2 contents (56.6–72.3 wt%), suggests that the final erupted magmas are derived from fractional crystallization of a mafic precursory magma displaying relatively consistent levels of crustal contamination. Andesites erupted between 4–3.7 ka and the 1995 eruption are contaminated to a greater extent, indicating that magmas with distinct compositions can feed phases of activity or individual eruptions. Post 1955 andesitic pyroclastics have lower SiO_2 and higher MgO than older lavas, yet equivalent Pb isotope ratios. The more mafic composition of post 1955 eruptive products can be attributed to increased throughput of mafic magma to the system.

✉ Joshua R. Brown
joshua.r.brown@durham.ac.uk

Rex N. Taylor
rex@soton.ac.uk

Masato Iguchi
iguchi.masato.8m@kyoto-u.ac.jp

[1] School of Ocean and Earth Science, University of Southampton, Waterfront Campus, European Way, Southampton SO14 3ZH, UK

[2] Sakurajima Volcano Research Center (SVO), Disaster Prevention Research Institute (DPRI), Kyoto University, Sakurajima-cho, Kagoshima-ken 891-1419, Japan

Introduction

Subduction zone magmas develop by addition of material from the downgoing slab to the mantle wedge (e.g. Armstrong 1971; Hawkesworth et al. 1993; Elliott 2004; Straub et al. 2010), with the resulting melts interacting with crustal lithologies in the overriding plate before eruption along the arc (e.g. Harmon et al. 1984; Hildreth and Moorbath 1988; Davidson et al. 2005; Ducea et al. 2015). Quantifying the proportions and identifying the origin of these slab, mantle and crustal components is important in understanding their roles in arc magma genesis. Isotopic studies provide a method of constraining these proportions and are key to defining where interaction occurs. Broad isotopic compositions of slab, mantle and crust are recognized (e.g. Dupré and Allègre 1983; Taylor and Maclennan 1985; Asmerom and Jacobsen 1993; Plank and Langmuir 1998; Workman and Hart 2005; Straub et al. 2010), but subtle changes in radiogenic isotopes have the potential to provide new information on the development and dynamics of sub-arc magma reservoirs.

Arc magmas often show temporal variation in radiogenic isotopic composition, both along arc and at individual volcanic centres, which can be related to changing contributions of mantle, slab and crustal components in their petrogenesis (e.g. Elburg and Foden 1998; Gómez-Tuena et al. 2003; Hanyu et al. 2006; Labanieh et al. 2010; Straub et al. 2015; Ishizuka et al. 2015). Recent advances in measurement precision of Pb isotopes allow subtle differences to be determined (e.g. Abouchami et al. 2000; Cassidy et al. 2012; Taylor et al. 2015), offering a means of assessing temporal changes in magmatic processes in greater detail. Despite this, relatively few studies have used high-resolution Pb isotopes in arcs to examine short-term processes (within a few thousand years and shorter timespans). Even minor variations in Pb isotopes can reveal the presence and interaction of compositionally distinct magmas beneath arc volcanoes over time (e.g. Cassidy et al. 2012; Kayzar et al. 2014; Ishizuka et al. 2015), which may correlate with surface activity. In this study, we utilize high-resolution Pb isotope analysis, complemented by major and trace element data, to probe short timescale changes in petrogenetic processes and magma-crust interaction at Sakurajima-Aira caldera volcano, of the Ryukyu arc in southern Japan.

Existing isotopic studies of Sakurajima-Aira and the Ryukyu arc suggest that erupted magmas are affected by crustal contamination (Hosono et al. 2008; Shibata et al. 2013a). However, the nature of the assimilant is poorly constrained at Sakurajima-Aira (Shibata et al. 2013a) as is the degree of assimilation and if/how this varies between eruptions. Majority of Sakurajima's eruptive history is characterized by intermittent Plinian and effusive eruptions, with a change in activity style to frequent Vulcanian explosions beginning in 1955 (Nakagawa et al. 2011; Iguchi 2013). This transition is suggestive of a change in processes in the magma plumbing system (Nakagawa et al. 2011).

Several studies have measured major and trace element, and Sr-Nd isotope compositions at Sakurajima, but few have examined in detail the Pb isotopic systematics. These were measured in 14 samples erupted between 29 ka and 2015, as well as for two nearby basalts. Pb isotope data for local crustal rocks is also presented to provide more accurate constraints on the components contributing to the isotopic signature of the samples. Although post 1955 eruptive products have been studied in terms of phenocryst composition (e.g. Nakagawa et al. 2011; Ebihara et al. 2013), there is little geochemical data available for this phase of eruptive activity. This is addressed here by the inclusion of four post 1955 samples. Comparison of the isotopic and elemental data from the post 1955 eruptions with the older volcanism is used for two aims: (1) to constrain crustal assimilation in terms of components, extent of contamination and temporal variation in these parameters and (2) to investigate whether petrogenetic processes occurring prior to more frequent post 1955 eruptions and older eruptions differ.
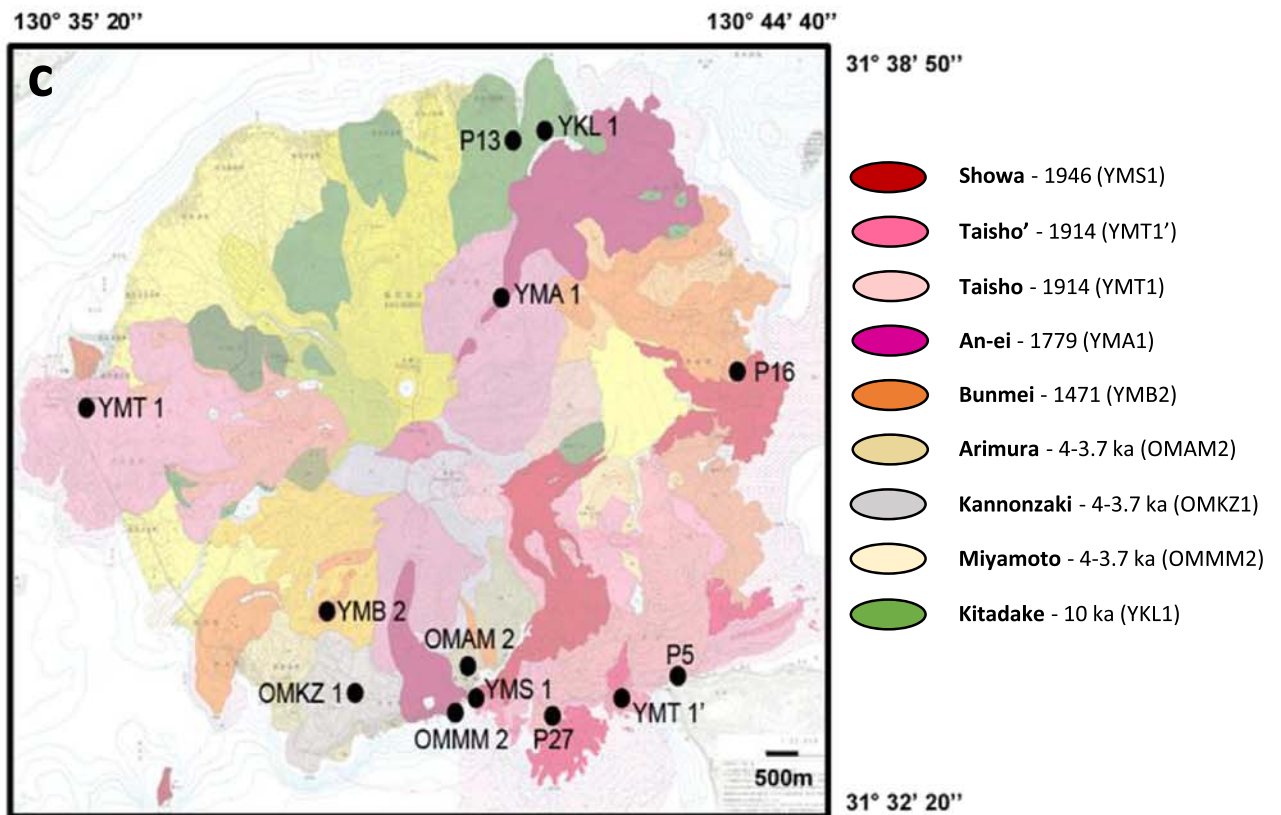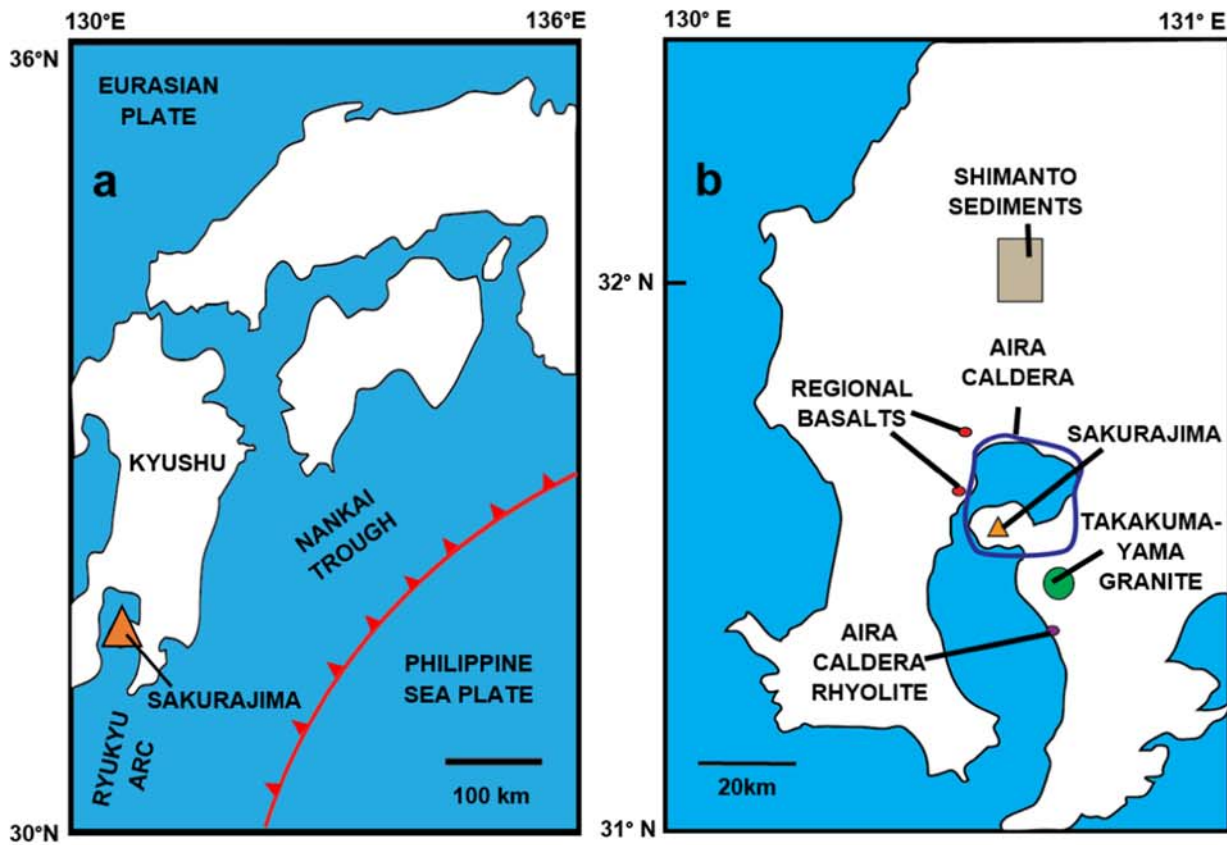
Geological setting and previous geochemical studies

Sakurajima is an active stratovolcano in southern Kyushu, Japan, located on the southern rim of the Aira caldera within the Kagoshima graben (Fukuyama 1978; Aramaki 1984). The Aira caldera forms part of the northern end of the Ryukyu arc, which exists due to the subduction of the Philippine Sea Plate (PSP) below the Eurasian Plate (Fukuyama 1978), as shown in Fig. 1. Volcanic activity has occurred in the region throughout the Quaternary, with the formation of Aira caldera in a cataclysmic eruption around 29 ka (Aramaki 1984). The Sakurajima edifice began to form around 26 ka (Takahashi et al. 2013) and has been through several phases of eruptive activity.

This study covers three phases of Sakurajima's eruptive history: the Younger Kitadake, Older Minamidake and Younger Minamidake stages. The Younger Kitadake dacite lavas were extruded around 10 ka (Takahashi et al. 2013). The andesitic Miyamoto, Kannonzaki and Arimura lavas were erupted during the Older Minamidake phase from 4 to 3.7 ka (Miki 1999). Notable eruptions in the Younger Minamidake phase include the 1471–1476 Bunmei and 1779–1782 An-ei dacitic lava flows. The most recent major eruption was the 1914–1915 Taisho event which produced two phases of andesitic lava flows. Secondary lava flows with a distinct chemical signature were derived from the flow fronts of the T1 and T2 lavas (Yanagi et al. 1991), forming the T1' and T2' lavas respectively. In 1946, the andesitic Showa lavas were erupted from the newly formed Showa crater (Takahashi et al. 2013). From 1955 to the present day, Vulcanian explosions have continued to occur at the Minamidake and Showa craters (Iguchi 2013).

Shibata et al. (2013a) sampled 22 volcano-stratigraphic units from Sakurajima, along with nearby basalts. Their study found no significant differences in the petrology of the eruptive products of Sakurajima, other than compositional variation from andesites to dacites. These were summarized as porphyritic with hyalo-ophitic groundmasses, containing clinopyroxene, orthopyroxene, plagioclase and opaque phenocrysts. Olivine phenocrysts were present in the basalts.

Fig. 1 **a** Tectonic map of southern Japan, showing the location of Sakurajima at the northern end of the Ryukyu arc. Modified from Shibata et al. (2013a). **b** Sampling sites of basalts and Aira caldera rhyolite relative to Aira caldera and Sakurajima volcano. Also shown are the sampling sites for the crustal materials considered in this study (the Shimanto sediments and Takakumayama granite). Location of Shimanto sediment samples after Hosono et al. (2008). Location of Takakumayama granite after Ishihara and Chappell (2010). Map modified from Hosono et al. (2008). **c** Sampling sites of the eruptive products of Sakurajima volcano, superimposed on the geological map of the volcano published by Kobayashi et al. (2013). Lava flow units sampled and associated sample names are listed in the legend. Pyroclastic samples collected from eruption fallout at time of eruption

a Map showing the Eurasian Plate, Kyushu, Nankai Trough, Philippine Sea Plate, Ryukyu Arc, and Sakurajima.

b Map showing Shimanto Sediments, Aira Caldera, Sakurajima, Regional Basalts, Takakuma-Yama Granite, and Aira Caldera Rhyolite.

c Geological map with sample locations: P13, YKL 1, YMA 1, P16, YMT 1, YMB 2, OMAM 2, OMKZ 1, YMS 1, OMMM 2, P27, P5, YMT 1'.

Legend:
- Showa – 1946 (YMS1)
- Taisho' – 1914 (YMT1')
- Taisho – 1914 (YMT1)
- An-ei – 1779 (YMA1)
- Bunmei – 1471 (YMB2)
- Arimura – 4–3.7 ka (OMAM2)
- Kannonzaki – 4–3.7 ka (OMKZ1)
- Miyamoto – 4–3.7 ka (OMMM2)
- Kitadake – 10 ka (YKL1)

Shibata et al. (2013a) measured Sr-Nd-Pb isotope ratios in eight samples from Sakurajima and two basalts. They found that the monogenetic maar volcano (Sumiyoshiike) basalts had Zr/Nb ratios close to those of MORB, and suggested that the mantle wedge below Sakurajima is of MORB-type mantle. Analysis of Sr, Nd and Pb isotopic compositions showed that the samples plot close to a mixing curve between MORB and sediments of the PSP. This led them to conclude that fluids are added to the regional mantle wedge from subducting PSP sediments. They inferred that the Sumiyoshiike basalts represent the primary magma of Sakurajima volcano because they plot almost on the MORB-PSP sediment mixing curve. The Sr-Nd-Pb isotopes of Sakurajima were found to lie off the mixing curve, displaying a more radiogenic signature. Shibata et al. (2013a) suggested this is due to the incorporation of crustal material, such as the locally exposed Shimanto sediments, into Sakurajima's magmas.

Medium-K volcanic rocks from across southern Kyushu form linear arrays between Sr-Nd and Pb-Pb isotopes (Hosono et al. 2008), indicative of mixing between a depleted, less radiogenic component (DC) and an enriched, more radiogenic component (EC). They proposed that Southern Kyushu volcanics acquire their isotopic signature via assimilation of both lower crustal material and Shimanto sediments (which together make up their enriched component) by basaltic mantle melts (the depleted component). They assume the lower crust to be of granodioritic composition based on seismic evidence from Iwasaki et al. (1990). Hosono et al. (2008) also suggest that silicic magmas of Southern Kyushu formed via fractional crystallization of the parent magma following assimilation. This is based on the relationship between isotopic and major element data, where silicic samples lie further away from the DC-EC mixing line.

Takahashi et al. (2013) measured major and trace element compositions of rhyolites from the 29 ka Aira caldera eruption together with basaltic andesite mafic inclusions, and Sakurajima andesites and dacites. They observed a wide range of incompatible trace element ratios and suggested that these could be produced by the mixing of mafic magma, represented by the inclusions, and the 29 ka rhyolitic magma. Uto et al. (2005) showed that magmas erupted since 2 ka have $^{87}Sr/^{86}Sr$, Nb/Th and Zr/Th ratios closer to basaltic inclusions than older eruptive products, indicating a recent trend towards more mafic compositions.

Examination of phenocrysts from the Bunmei, An-ei, Taisho and Showa eruptions by Yanagi et al. (1991) showed that the Taisho and Showa lavas contain plagioclase with bimodal An compositions. This led them to propose that prior to the 1914 Taisho and 1946 Showa eruptions, dacitic magma with low-An plagioclase was mixed with high-An plagioclase basaltic magma. Nakagawa et al. (2011) reported the presence of olivine phenocrysts (derived from basaltic magma) in post 1955 eruptive products. This led them to suggest that recent activity has been driven by the injection of basaltic magma, and that this is the cause of increased eruption frequency since 1955.

Methods

The eruptive products of Sakurajima are divided into andesites, dacites and post 1955 andesites, to distinguish the andesitic pyroclastics erupted since 1955 from the older andesitic and dacitic lava flows. Figure 1 shows the sampling sites for the eruptive products of Sakurajima. Locations of local crustal materials (Shimanto sediments and Takakumayama granite), regional basalts (Sumiyoshiike and Shirahama basalts, also used in the isotopic study of Shibata et al. 2013a) and the Aira caldera rhyolite are also shown in Fig. 1. Rock samples were crushed inside polyethylene bags using a fly press. The crushed material was then separated using a Teflon sieve to isolate 0.5–1-mm chips. This fraction was repeatedly rinsed with 18 MΩ water before cleaning in an ultrasonic bath for 10 min. Chips were examined under a binocular microscope to ensure only uncontaminated material progressed to analysis. All measurements were conducted at the School of Ocean and Earth Science, University of Southampton, UK.

Major elements

Selected rock chips were powdered in an agate pestle and mortar, placed in a crucible and dried overnight at 105 °C. Loss on ignition was determined via heating in a furnace at 1000 °C for 4 h. The cooled powders were then mixed with $LiBO_4$ (10:1 $LiBO_4$:rock powder) and fused into glass beads, as per the methods of Croudace and Williams-Thorpe (1988). Whole rock major element compositions were measured using WD-XRF, using a Philips Mag-Ix-Pro XRF spectrometer calibrated using international rock standards. The uncertainty on the XRF measurements is less than 1% for all elements (see Appendix B for reproducibility using standard BRR1).

Trace elements

An aliquot of clean selected chips was powdered and digested with HNO_3:HF. Daughter solutions were 4000:1 dilutions and were spiked with a Be-In-Re internal standard prior to measurement. Trace elements were measured by inductively coupled plasma mass spectrometry (ICP-MS) using a Thermo Scientific X-Series II. Measurements were corrected for interferences and blank, then calibrated using a suite of international rock standards (JB-3, JB-1a, JGb-1, BHVO-2, BIR-1, JA-2, reference data from GeoReM database, Jochum et al. 2005) and in-house reference materials. Long-term accuracy relative to reference values is 3–5%.

Table 1 Major element oxide concentrations, in wt% oxide, and trace element concentrations, in ppm, for the 16 samples measured. *YE* year erupted

	YMA1	YMB2	YKL1	OPF1	SYB	SHB1	P27	P5	P13	P16	OMKZ1	OMAM2	OMMM2	YMS1	YMT1	YMT1'
Age (ka)	0.239	0.547	10	29	7.2	930	2015 (YE)	1978 (YE)	1995 (YE)	2000 (YE)	4–3.7	4–3.7	4–3.7	0.072	0.104	0.104
Composition	Dacite	Dacite	Dacite	Rhyolite	Basalt	Basalt	Post 1955 andesite	Post 1955 andesite	Post 1955 andesite	Post 1955 andesite	Andesite	Andesite	Andesite	Andesite	Andesite	Andesite
SiO_2 (wt%)	62.95	62.82	64.42	72.27	46.74	48.63	57.25	57.91	56.60	60.41	61.39	60.32	58.32	59.68		60.67
TiO_2	0.79	0.75	0.65	0.24	1.03	0.91	0.76	0.81	0.72	0.75	0.74	0.75	0.72	0.78		0.79
Al_2O_3	16.11	16.85	16.21	14.91	17.71	19.20	17.20	16.77	18.03	17.03	16.78	16.42	17.37	16.93		16.33
Fe_2O_3	6.48	5.99	5.54	2.54	13.02	11.69	8.23	8.31	7.86	7.07	7.38	7.57	7.51	7.32		7.27
MnO	0.14	0.13	0.13	0.07	0.20	0.19	0.16	0.16	0.15	0.13	0.16	0.16	0.15	0.15		0.15
MgO	1.67	1.57	1.73	0.47	6.23	6.31	3.69	3.27	3.22	2.50	2.75	2.62	2.94	2.60		2.36
CaO	5.27	5.70	5.05	3.12	11.47	11.14	7.87	7.14	8.12	6.78	6.28	5.87	7.15	6.78		6.16
K_2O	1.95	1.94	2.07	2.49	0.38	0.38	1.28	1.41	1.25	1.61	1.73	1.73	1.46	1.56		1.68
Na_2O	3.77	3.67	3.56	3.60	2.13	2.35	2.98	3.17	3.05	3.09	3.25	3.24	3.13	3.36		3.52
P_2O_5	0.20	0.17	0.14	0.05	0.11	0.16	0.14	0.15	0.14	0.17	0.14	0.14	0.14	0.17		0.18
Total	99.33	99.60	99.51	99.76	99.01	100.96	99.55	99.10	99.13	99.54	100.58	98.80	98.90	99.31		99.11
Li (ppm)	26.1	9.1	18.5	22.1	5.2	7.6	18.3	17.1	13.6	17.1	18.6	22.7	20.3	19.1	20.1	21.5
Sc	16.71	18.03	14.87	9.31	47.31	42.50	26.61	26.27	30.43	23.02	18.80	23.07	23.08	27.38	19.12	25.86
Ti	3893	3858	2953	2345	6593	5607	4691	4259	3980	4624	2568	4279	4056	4634	4313	4552
V	51.0	65.9	50.9	43.7	420.3	324.7	161.9	162.2	179.5	123.3	86.7	135.3	127.2	156.2	104.8	121.2
Cr	25.8	3.4	2.5	2.6	10.0	40.8	7.3	8.0	12.5	4.9	7.6	7.5	15.9	6.8	3.5	4.0
Co	5.37	7.04	5.61	4.19	39.33	32.13	16.91	17.37	19.41	13.53	9.47	12.22	12.16	14.71	9.37	11.90
Ni	24.9	1.7	2.0	1.0	15.7	16.5	5.4	4.8	6.4	3.8	2.6	3.4	4.6	3.5	2.3	4.7
Cu	6.72	4.25	8.94	1.80	52.85	38.38	22.16	17.85	17.55	20.18	10.05	15.63	14.20	11.84	11.06	14.20
Zn	69.10	66.91	55.67	59.87	97.55	92.52	79.67	83.82	77.68	81.96	58.95	79.03	70.72	80.15	70.61	80.47
Rb	67.05	60.30	79.29	48.84	8.77	5.76	47.83	37.51	27.15	63.84	44.14	66.19	63.23	44.74	55.37	55.05
Sr	262.9	277.5	255.6	274.0	341.9	480.7	284.3	316.0	336.9	260.1	338.4	230.0	239.3	303.1	241.4	271.1
Y	30.32	27.76	24.98	11.52	21.80	20.67	25.83	19.91	16.70	29.84	19.01	26.38	26.97	23.52	26.39	27.83
Zr	141.9	127.6	136.3	46.7	42.5	65.0	105.9	80.1	60.1	121.3	84.4	125.5	125.9	96.2	118.4	118.1
Nb	6.90	6.01	6.99	5.24	3.46	2.34	5.03	3.84	2.88	5.99	4.18	6.27	6.18	4.58	5.62	5.62
Cs	4.04	3.61	3.20	3.01	0.36	0.66	2.83	2.22	1.60	3.76	2.57	3.87	3.68	2.66	3.32	3.26
Ba	328.1	297.5	376.4	276.4	99.7	120.5	242.7	197.5	152.4	286.2	229.1	298.3	293.9	228.2	271.8	2732.3
La	18.78	16.89	19.79	14.32	5.43	7.02	14.27	11.32	8.73	16.83	12.95	17.18	16.87	13.26	15.86	15.99
Ce	41.06	36.95	40.76	27.24	13.01	17.48	31.65	24.69	19.13	37.33	27.42	37.32	36.63	29.21	34.88	35.28
Pr	4.96	4.54	4.71	2.95	1.96	2.60	3.96	3.06	2.39	4.64	3.26	4.42	4.41	3.62	4.27	4.32
Nd	20.08	18.36	18.24	10.59	9.50	12.08	16.42	12.61	10.03	19.13	13.05	17.78	17.69	14.99	17.42	17.87
Sm	4.69	4.28	3.96	2.07	2.82	3.18	3.91	3.01	2.45	4.51	3.02	4.07	4.14	3.56	4.11	4.23
Eu	1.28	1.18	1.14	1.05	1.00	1.05	1.09	1.00	0.89	1.22	1.10	1.03	1.05	1.10	1.10	1.19

Table 1 (continued)

	YMA1	YMB2	YKL1	OPF1	SYB	SHB1	P27	P5	P13	P16	OMKZ1	OMAM2	OMMM2	YMS1	YMT1	YMT1'
Gd	4.78	4.36	3.89	1.87	3.36	3.43	4.16	3.16	2.64	4.72	3.06	4.15	4.23	3.75	4.24	4.40
Tb	0.79	0.72	0.64	0.30	0.56	0.55	0.67	0.52	0.44	0.77	0.50	0.68	0.70	0.62	0.69	0.72
Dy	4.86	4.50	3.99	1.84	3.58	3.45	4.20	3.24	2.75	4.81	3.12	4.30	4.36	3.84	4.30	4.54
Ho	1.04	0.95	0.84	0.39	0.76	0.73	0.89	0.69	0.59	1.02	0.66	0.91	0.92	0.81	0.91	0.96
Er	3.01	2.77	2.50	1.13	2.19	2.08	2.58	2.01	1.68	2.95	1.91	2.66	2.68	2.36	2.66	2.79
Tm	0.46	0.42	0.39	0.17	0.33	0.31	0.39	0.30	0.25	0.44	0.29	0.41	0.41	0.35	0.40	0.42
Yb	3.07	2.81	2.58	1.21	2.12	2.00	2.56	2.05	1.70	2.96	1.94	2.72	2.76	2.36	2.68	2.81
Lu	0.47	0.43	0.40	0.19	0.31	0.30	0.39	0.31	0.26	0.45	0.30	0.42	0.42	0.36	0.41	0.43
Hf	3.71	3.38	3.69	1.37	1.28	1.78	2.86	2.16	1.62	3.23	2.25	3.32	3.31	2.55	3.16	3.13
Ta	0.69	0.50	0.63	0.42	0.29	0.14	0.42	0.32	0.24	0.49	0.37	0.54	0.51	0.38	0.47	0.46
Pb	13.28	11.37	14.42	11.02	2.19	4.33	9.37	7.87	6.02	9.21	9.46	13.12	12.19	9.08	19.64	11.37
Th	6.36	5.80	7.50	4.59	0.82	1.23	4.57	3.54	2.53	5.50	4.09	6.19	5.96	4.15	5.23	5.13
U	1.48	1.35	1.70	1.01	0.20	0.29	1.06	0.82	0.60	1.29	0.95	1.42	1.36	0.97	1.22	1.20

Pb isotopes

Pb was separated in a class 100 clean laboratory in the University of Southampton using sub-boiled and ultra-pure Pb reagents. 0.4 g of rock chips was leached at 150 °C in 4 M HCl for 30 min, then repeatedly rinsed in pure water. Leached chips were then dissolved for more than 24 h in approximately 4 ml of an HF:HNO$_3$ (4:1) mixture. Pb was then isolated from the matrix using two passes through AG1x8, 200–400 mesh anion exchange resin using 0.5 M HBr and recovery in 10 M HCl. Pb isotopes were measured using a Thermo Neptune multi-collector inductively coupled plasma mass spectrometry (MC-ICP-MS). Samples were corrected for instrumental mass fractionation using the SBL74 double spike (Taylor et al. 2015). Immediately prior to measurement, the samples were split into a natural fraction and an aliquot spiked with the SBL74. The natural and doubled spiked fractions were run in separate batches separated by cleaning of the sample introduction system. Reproducibility of Pb isotope ratios was estimated based on 39 measurements of SRM NBS 981 run in 2017–2018. This produced average ratios of $^{206}Pb/^{204}Pb = 16.9402 \pm 0.0031$ (2σ), $^{207}Pb/^{204}Pb = 15.4964 \pm 0.0025$ (2σ) and $^{208}Pb/^{204}Pb = 36.7118 \pm 0.0073$ (2σ). Pb blanks are less than 85 pg.

Results

Major and trace elements

Compositions and ages of the samples used for this study are summarized in Appendix A. Whole rock major and trace element concentrations are listed in Table 1, with selected elements plotted on Harker diagrams in Fig. 2 and as a time series in Fig. 3. SiO$_2$ of Sakurajima ranges from 46.7 wt% in the basalts, through andesite and dacite, to 72.3 wt% in the rhyolite. Figure 2 shows CaO, Al$_2$O$_3$, Fe$_2$O$_3$ and MgO all decrease linearly with increasing SiO$_2$, while Na$_2$O and K$_2$O increase. TiO$_2$ contents (Fig. 2) show a general decline with increasing SiO$_2$, but are very similar for the andesites, dacites and post 1955 andesites, clustering between 0.65 and 0.81 wt%. P$_2$O$_5$ content is more variable across the range of SiO$_2$ contents (Fig. 2).

Variation in composition with time (Fig. 3) reveals that there has been a tendency for magmatism to become more mafic. Eruptions since 1955 have been predominantly pyroclastic with SiO$_2$ contents 56.6–60.4 wt%, slightly lower than pre-1955 andesitic lavas (57.9–61.4 wt%). Recent pyroclastics also have higher MgO at 2.5–3.7 wt% relative to 2.4–2.9 wt% in pre-1955 andesites.

Key incompatible trace element and rare-earth element concentrations, normalized to primitive mantle, are shown in Fig. 4. Similar profiles are observed across the

Fig. 2 Plots of SiO₂ vs major element oxides for the eruptive products of Sakurajima, Aira caldera and basalts. **a** CaO. **b** K₂O. **c** TiO₂. **d** Al₂O₃. **e** Na₂O. **f** P₂O₅. **g** Fe₂O₃. **h** MgO
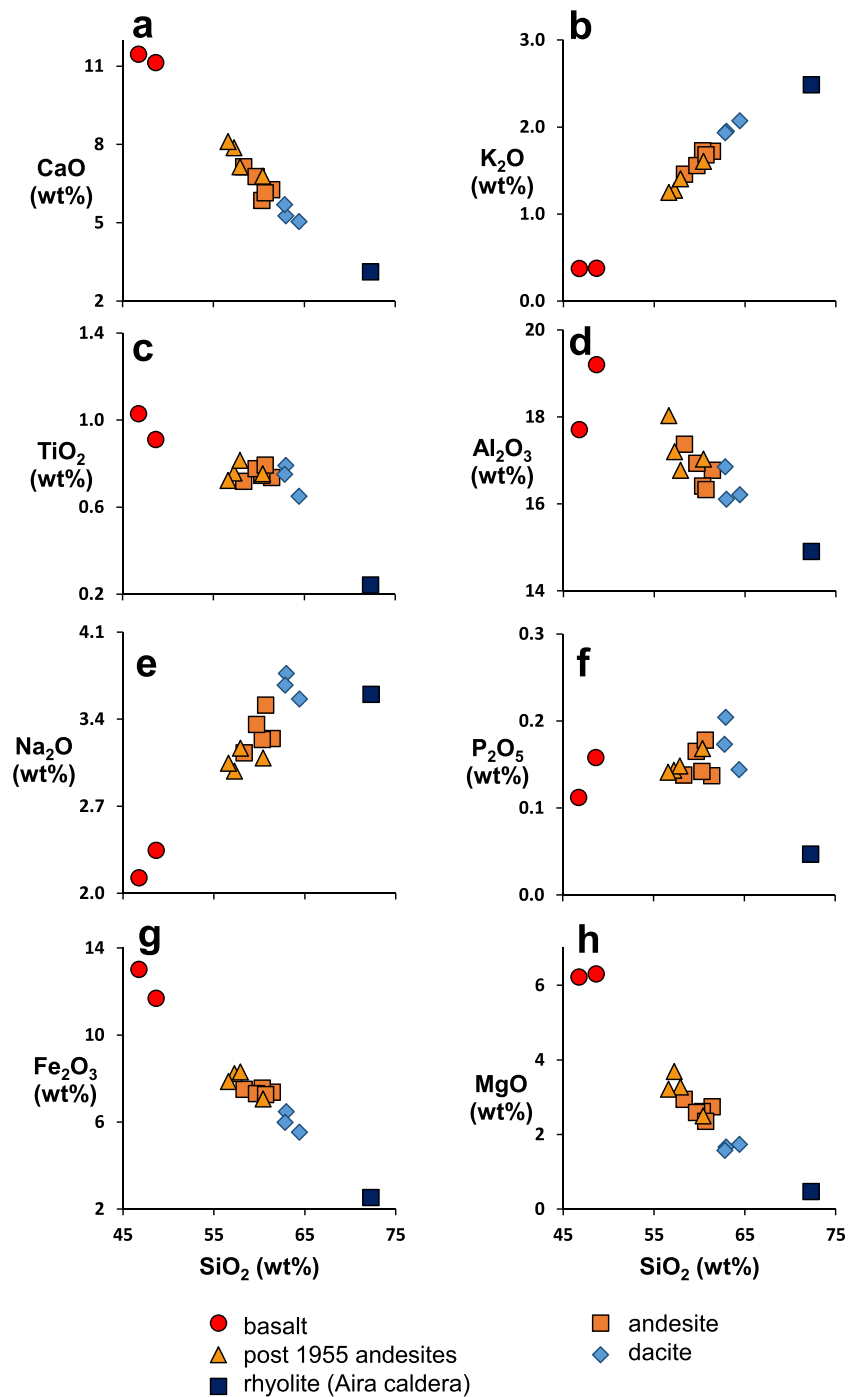

lithologies and have the characteristic island arc signature of Nb and Ta depletion and enrichment in LILE's, e.g. Cs, Rb and Pb, relative to the REE. All samples are progressively enriched in LREE's (La to Eu) and flat through the HREE (Dy–Yb). Very incompatible/moderately incompatible trace element ratios such as Ba/La, U/Pb and Dy/Yb are all consistent through the basalt-to-rhyolite sequence. One difference observed between the basalts and the andesites/dacites is that they are less enriched in Cs, Rb and K relative to Ba.

Pb isotopes

High-resolution Pb isotope data for Sakurajima is presented in Table 2. As all samples (other than the Shirahama basalt) were erupted in the last 30,000 years, no age correction was applied to the data. Overall, Sakurajima forms linear arrays in $^{207}Pb/^{204}Pb$ vs $^{206}Pb/^{204}Pb$ and $^{208}Pb/^{204}Pb$ vs $^{206}Pb/^{204}Pb$ (Fig. 5) which plot significantly above the NHRL with Δ7/4Pb and Δ8/4Pb of ~ 12 and 76 respectively. The basalts have less radiogenic Pb

Fig. 3 Plots of **a** SiO₂ vs age and **b** MgO vs age, for the eruptive products of Sakurajima. The years of post 1955 eruptions are labelled. Smaller grey symbols show published data from Shibata et al. (2013a)—circles, Takahashi et al. (2013)—triangles, and Matsumoto et al. (2013)—squares
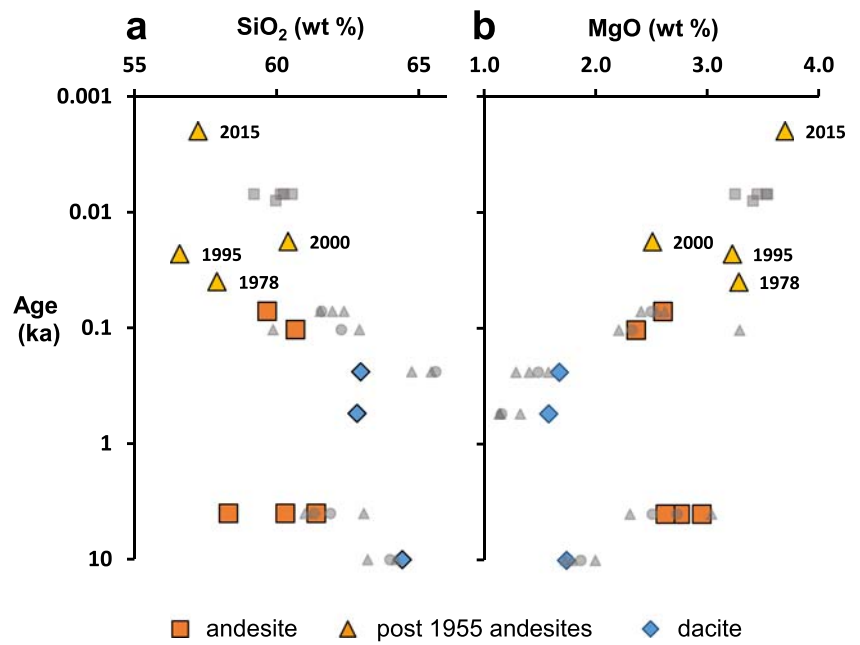
Fig. 4 Primitive mantle normalized trace element compositions for **a** Aira caldera rhyolite and dacites, **b** andesites and **c** basalts. Normalizing values from Sun and McDonough (1989)
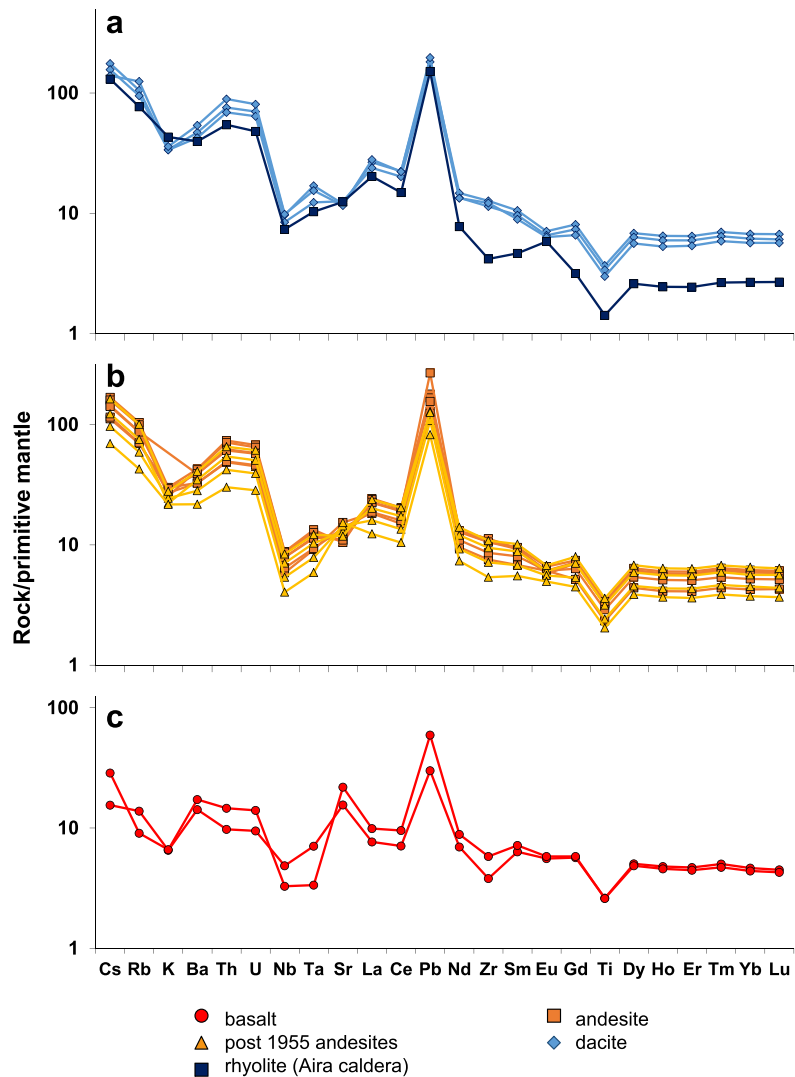
Table 2 Pb isotope ratios and delta Pb values for the 16 samples measured. $\Delta 7/4$ Pb and $\Delta 8/4$ Pb values calculated using the methods of Hart (1984). *YE* year erupted

	YMA1	YMB2	YKL1	OPF1	SYB	SHB1	P27	P5	P13	P16	OMKZ1	OMAM2	OMMM2	YMS1	YMT1	YMT1'
Age (ka)	0.239	0.547	10	29	7.2	930	2015 (YE)	1978 (YE)	1995 (YE)	2000 (YE)	4–3.7	4–3.7	4–3.7	0.072	0.104	0.104
Composition	Dacite	Dacite	Dacite	Rhyolite	Basalt	Basalt	Post 1955 andesite	Post 1955 andesite	Post 1955 andesite	Post 1955 andesite	Andesite	Andesite	Andesite	Andesite	Andesite	Andesite
$^{206}Pb/^{204}Pb$	18.4053	18.4019	18.4034	18.3992	18.2440	18.2699	18.3997	18.4027	18.4207	18.4043	18.4142	18.4166	18.4098	18.4033	18.4010	18.4000
$^{207}Pb/^{204}Pb$	15.6069	15.6049	15.6059	15.6045	15.5482	15.5576	15.6043	15.6054	15.6126	15.6078	15.6092	15.6087	15.6048	15.6057	15.6022	15.6020
$^{208}Pb/^{204}Pb$	38.6442	38.6366	38.6396	38.6441	38.3117	38.3651	38.6325	38.6397	38.6774	38.6462	38.6593	38.6590	38.6436	38.6409	38.6292	38.6264
$\Delta 7/4$ Pb	12.1	11.9	12.0	11.9	8.0	8.6	11.9	12.0	12.5	12.2	12.2	12.1	11.8	12.0	11.7	11.6
$\Delta 8/4$ Pb	76.5	76.2	76.3	77.3	62.8	65.0	76.0	76.4	78.0	76.8	77.0	76.6	75.9	76.4	75.5	75.4

isotope ratios than the more evolved rocks, with the Sumiyoshiike basalt having the lowest ratios of $^{206}Pb/^{204}Pb = 18.24$, $^{207}Pb/^{204}Pb = 15.55$ and $^{208}Pb/^{204}Pb = 38.31$. Sakurajima and the Aira caldera rhyolites have very similar Pb isotope ratios with $^{206}Pb/^{204}Pb$ ~ 18.40–18.42. When viewed at a finer scale (Fig. 5), the Pb isotope data shows that andesites erupted between 4 and 3.7 ka and in 1995 plot to more radiogenic compositions than the remaining samples.

Discussion

Crustal assimilation and fractional crystallization

As basalts have not erupted or been recorded from Sakurajima, the composition of the unfractionated magmas is difficult to measure directly. In this case, we utilize basalts erupted in the vicinity of Sakurajima volcano as a proxy for primitive magma compositions feeding the system. The Sumiyoshiike basalts erupted at 7.2 ka (Shibata et al. 2013a) are found less than 4 km outside the Aira caldera (see Fig. 1) and hence may represent eruptions that have bypassed the Sakurajima magma reservoir. An alternative is the Shirahama basalts, which make up a significant component of the volcanism in the area before the formation of Aira caldera, potentially representing mafic magmas from a less mature, more primitive volcanic system. Although these two regional basalts have similar elemental and isotopic compositions, the Shirahama basalt lies outside the age range of Aira-Sakurajima volcanism. On this basis, we have chosen the Sumiyoshiike basalts as the best primitive magma proxy. Their inclusion in a sample set of mafic magmas from Southern Kyushu deemed to have been negligibly affected by shallow crystallization and contamination processes (Shinjo et al. 2000) further support this.

In comparison to the Sumiyoshiike basalts, the eruptive products of Sakurajima (hereon taken to include the Aira caldera rhyolite) have more radiogenic Pb (Fig. 5). This suggests that the Sumiyoshiike basalts and Sakurajima magmas are either derived from mantle sources with different levels of subduction addition or have experienced variable amounts of assimilation of radiogenic crust. To distinguish between these two possibilities, we have examined the Pb isotope systematics of these magmas in relation to mantle, subduction and crustal components in Fig. 6. Subducting sediments and the Philippine Sea ocean crust have been well characterized by drilling and dredging (Hickey-Vargas 1998; Shimoda et al. 1998) while the mantle wedge is constrained from numerous studies across the Philippine Plate and Japan Sea as being a variant of Indian Ocean MORB (e.g. Pouclet et al. 1994; Hickey-Vargas 1998). Upper crust beneath Sakurajima is

Fig. 5 Plots of **a, b** ^{207}Pb/^{204}Pb vs ^{206}Pb/^{204}Pb and **c, d** ^{208}Pb/^{204}Pb vs ^{206}Pb/^{204}Pb, for the eruptive products of Sakurajima, Aira caldera and basalts. The Northern Hemisphere Reference Line (NHRL) was calculated using the equations of Hart (1984). Plots **b** and **d** are higher resolution versions of **a** and **c** respectively. The error ellipse is calculated using starting values of ^{206}Pb/^{204}Pb = 18.4207, ^{207}Pb/^{204}Pb = 15.6126 and ^{208}Pb/^{204}Pb = 38.6774. The ellipse is based on the reproducibility of Pb isotope ratios quoted in the "Methods" section

- ● basalt
- ▲ post 1955 andesites
- ■ rhyolite (Aira caldera)
- ■ andesite
- ◆ dacite
- — NHRL
- ⬭ Error ellipse
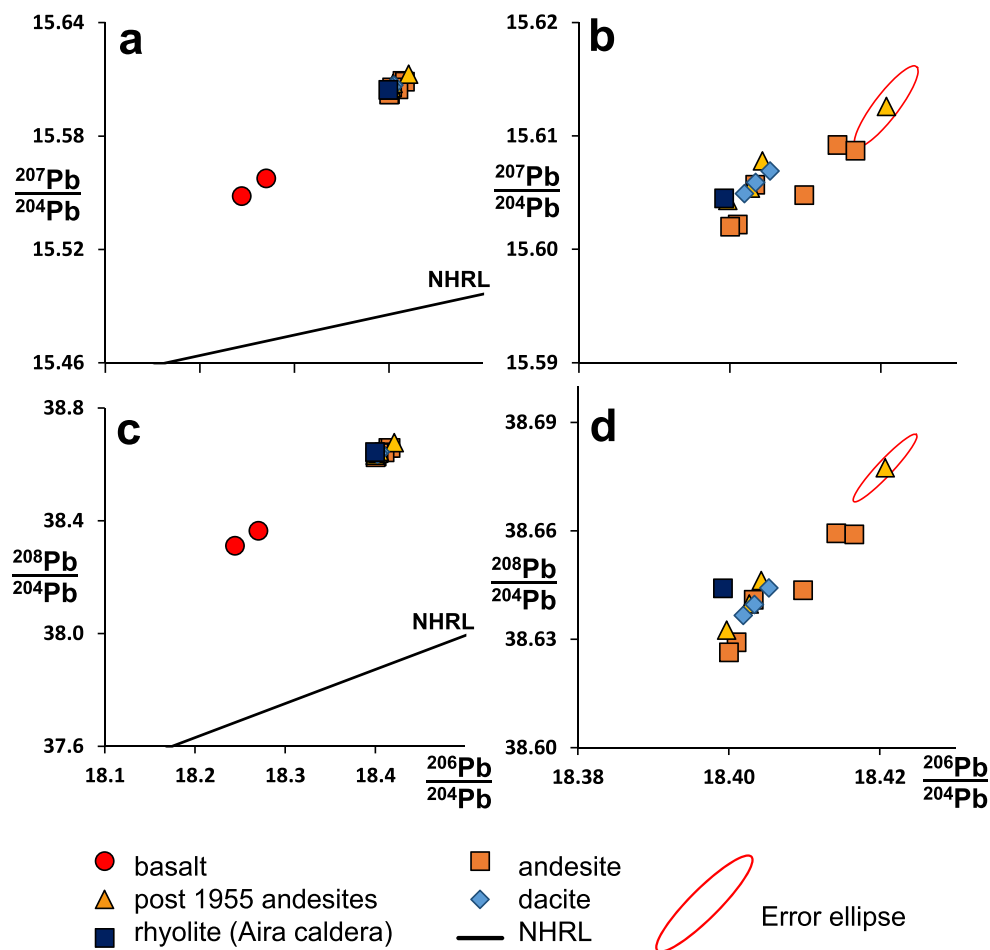
composed of the Shimanto supergroup sediments, while the lower crust is composed of Miocene granitoids (Hosono et al. 2008). This is supported by seismic studies that indicate a granodioritic lower crustal composition beneath Southern Kyushu (Iwasaki et al. 1990). The Takakumayama granite is a middle Miocene granite exposure located less than 25 km south-east of Sakurajima (Matsui 2006; Ishihara and Chappell 2010), and this is used here to represent the lower crustal composition beneath Sakurajima.

From Figs. 6 and 7, it is apparent that there is an essentially linear trend of progressively more radiogenic compositions through the sequence: basalts, Aira, Sakurajima, Takakumayama granite and Shimanto sediments. This suggests that incorporation of lower crustal granitic or Shimanto sedimentary material into the basaltic magma could result in the Pb isotope compositions of Sakurajima. In contrast, the subducted PSP sediments are not collinear with this sequence and lie to lower Δ7/4Pb and Δ8/4Pb at higher ^{206}Pb/^{204}Pb (Fig. 6).

Figure 7 shows a mixing line between Sumiyoshiike basalt and "average crust" (estimated as 50% Takakumayama granite, 50% average Shimanto sediments) below Sakurajima. Incorporation of crustal materials into magmas can occur via

direct assimilation of crustal xenoliths, or incorporation and mixing of a partial melt of the crust (Grove et al. 1988). Due to the lack of xenoliths in Sakurajima's eruptive products, the partial melting model (favoured by Kuritani et al. 2005; Ishizuka et al. 2017; and others) is utilized here. Figure 8 shows that Sakurajima samples plot within error of this mixing line, with their isotopic signature corresponding to the addition of 5–6% average crustal melt to the basaltic magma (see Appendix C for calculation of Pb concentration in crustal melt). Our high-precision analyses allow this mixing trend to be tightly constrained and differences in proportions of mixing components as low as 1% to be resolved. If assimilation of bulk crust is assumed, the amount of crustal material added increases to around 10%.

The Sumiyoshiike basalt is used as the mixing end member because it represents the best available proxy for primitive magmas feeding Sakurajima volcano. However, it could be argued that the intermediate position of the basalts between the mantle wedge and the crustal components in Fig. 6 indicates that the basalts are themselves affected by some degree of crustal contamination. The mixing line in Fig. 7 can be extrapolated further back to other less radiogenic compositions (red trend line on Fig. 6), suggesting that the
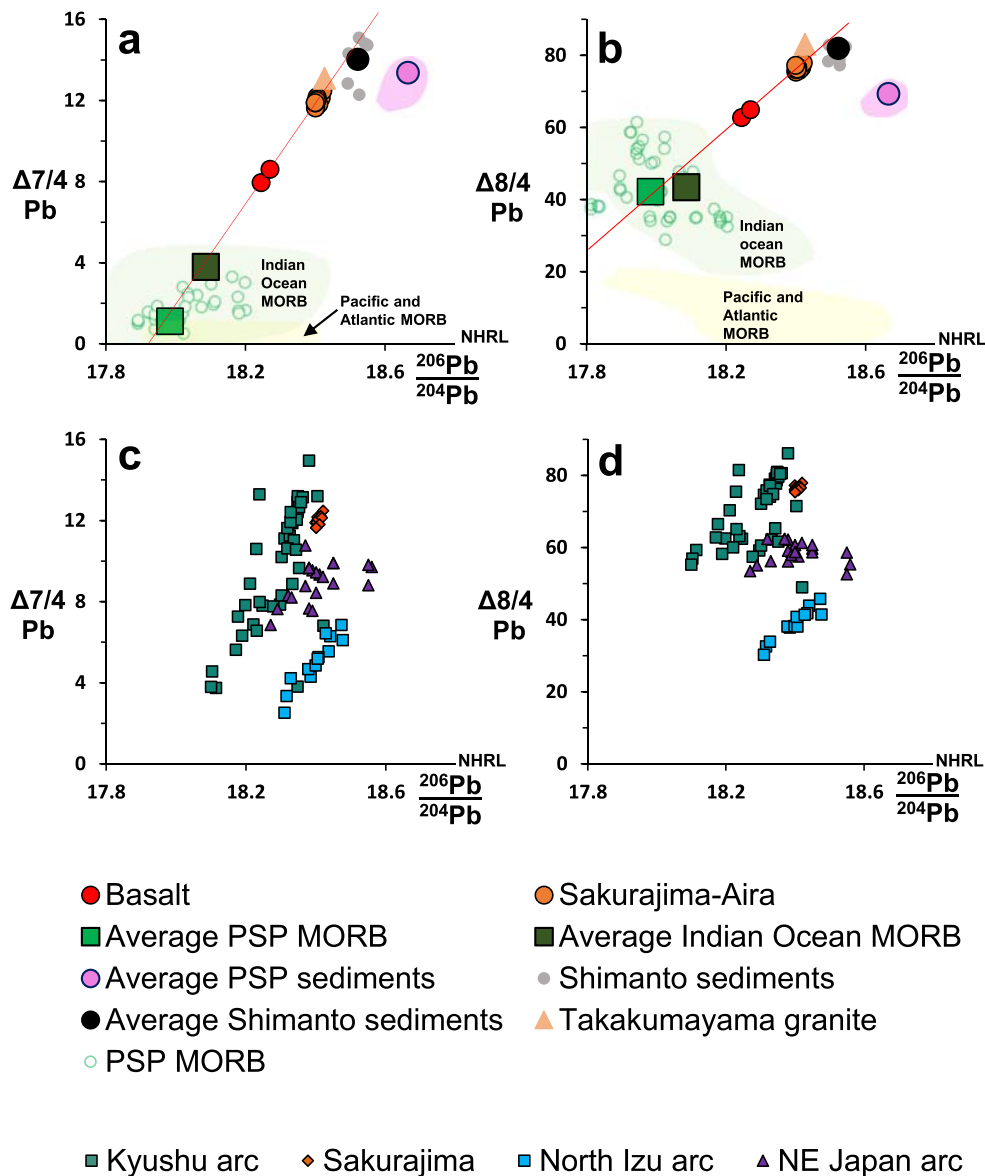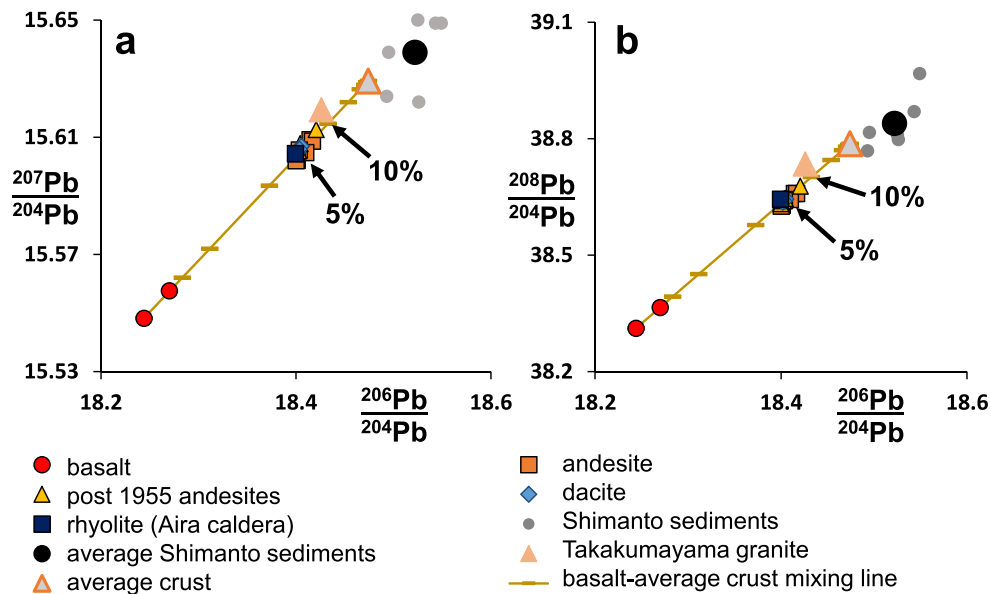
Fig. 6 Plots of **a** Δ7/4 Pb vs $^{206}Pb/^{204}Pb$ and **b** Δ8/4 Pb vs $^{206}Pb/^{204}Pb$, for the samples from this study along with mantle, subduction and crustal components. Sakurajima-Aira orange circles represent the andesites, post 1955 andesites, dacites and Aira caldera rhyolite from Fig. 5. Data sources: PSP sediments—average composition of samples from Shimoda et al. (1998). Range of compositions shown by pink field. PSP MORB—average composition from Ishizuka et al. (2009) and Ishizuka et al. (2010). Average Indian Ocean MORB—average composition from compiled data of Meyzen et al. (2007), excluding areas known to be contaminated by mantle plumes. Shimanto sediments—Hosono and Nakano (2003). Takakumayama granite—average composition of

samples from Shin (2008). Indian Ocean MORB field (green) and Pacific and Atlantic MORB field (yellow) based on data from Meyzen et al. (2007). Thin red trend line shows collinearity of basalts, Sakurajima-Aira samples and crustal compositions. Plots **c** and **d** show Δ7/4 Pb vs $^{206}Pb/^{204}Pb$ and Δ8/4 Pb vs $^{206}Pb/^{204}Pb$ respectively, for Sakurajima (orange) and volcanic arcs across Japan. Data sources: Kyushu arc—Shibata et al. (2013b), Hosono and Nakano (2003), Hosono et al. (2003); North Izu arc—Taylor and Nesbitt (1998); NE Japan arc—Hanyu et al. (2006). All Δ7/4 Pb and Δ8/4 Pb values, and NHRL (Northern Hemisphere Reference Line), calculated using the methods of Hart (1984)

Sumiyoshiike basalts represent primitive magma compositions produced by initial crustal contamination of primary mantle-derived magmas. These primary arc magmas may themselves lie amidst an array formed between subducted sediment, subducted ocean crust and the mantle wedge. Crustal addition estimated for the Sakurajima samples would therefore be accordingly greater if calculated using the less radiogenic mantle-derived magmas.

Mixing lines between basalt and granite, and basalt and average sediments do not overlap with sample error ellipses (Fig. 8), suggesting that addition of only one crustal component does not produce the sample compositions. It is noted that extrapolation of the basalt-average crust mixing line towards more radiogenic compositions causes it to pass through the compositional field defined by the Shimanto sediments (Fig. 8). However, the Shimanto sediments show considerable

Fig. 7 Plots of **a** ^{207}Pb/^{204}Pb vs ^{206}Pb/^{204}Pb and **b** ^{208}Pb/^{204}Pb vs ^{206}Pb/^{204}Pb, for the eruptive products of Sakurajima, Aira caldera, basalts and potential crustal components. Data sources: Shimanto sediments—Hosono and Nakano (2003). Takakumayama granite—average composition of samples from Shin (2008). Average crust represents a 50:50 mixture of average Shimanto sediments and Takakumayama granite. The Sumiyoshiike basalt sample is used as the basaltic end member for the basalt-average crust mixing line. Labelled tick marks on mixing line represent percentage of average crustal melt

isotopic heterogeneity, suggesting that their average may best represent a bulk composition. Explaining the Sakurajima isotope systematics by only adding Shimanto sediments would require a sediment composition different to any existing samples. Hence, "average crust" is considered the more appropriate mixing end member, with the resultant mixing line overlapping with almost all Sakurajima sample error ellipses in both ^{206}Pb/^{204}Pb-^{207}Pb/^{204}Pb and ^{206}Pb/^{204}Pb-^{208}Pb/^{204}Pb space (Fig. 8).

This assimilation model is consistent with Hosono et al. (2008), who proposed that the Sr-Nd-Pb isotopic signatures of volcanic rocks across Southern Kyushu result from contamination of mafic magma with lower crustal granodioritic and upper crustal sedimentary materials. Significant crustal contamination does not occur in the northern Izu arc (Taylor and Nesbitt 1998) and is not considered a major contributor to the Pb isotope signature of the North-East Japan arc (Hanyu et al. 2006). The higher Δ7/4Pb and Δ8/4Pb of Sakurajima and other Kyushu volcanoes compared to the North Izu and North-East Japan arcs (Fig. 6) is likely to be a product of a crustal signature superimposed on the supra-subduction primary magmas in this region.
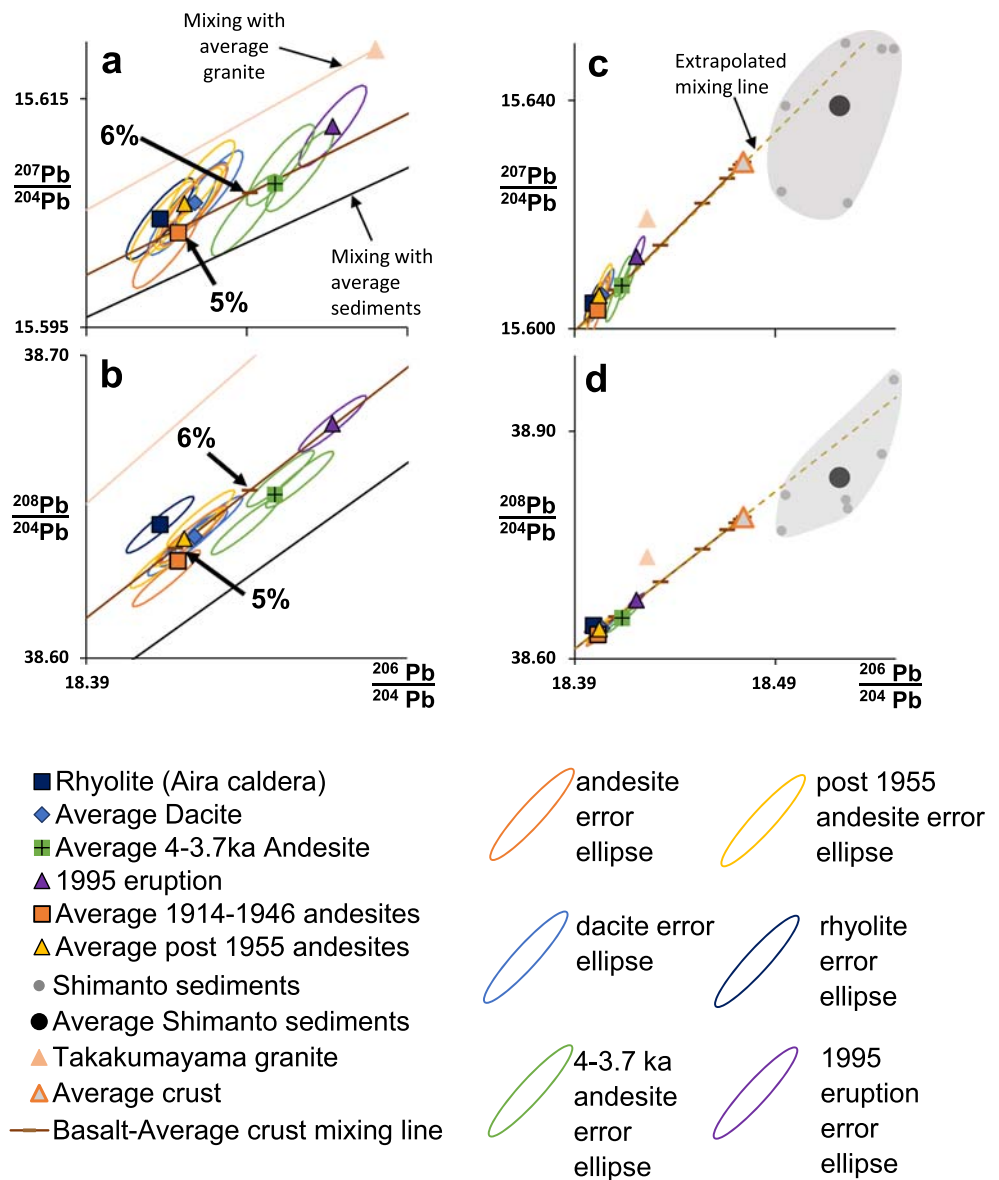
Figure 9 shows that, in general terms, Sakurajima has relatively consistent Pb isotope ratios (~ 18.4) through a range of SiO$_2$ and MgO. This is consistent with this suite of rocks being related by fractional crystallization from an isotopically similar precursory magma. The fractionation vectors on these plots project back to intersect the basalt-average crust mixing line at ~ 5% crustal melt. As the Sumiyoshiike basalts have

less radiogenic Pb than this intersection, it implies that they have experienced less crustal contamination than the precursory magma. In other words, the magma feeding directly into the upper crustal Sakurajima-Aira reservoir was likely to have been already contaminated deeper in the crust. This is again consistent with the model for Southern Kyushu volcanics proposed by Hosono et al. (2008), who suggested that higher silica rocks in the region formed via fractional crystallization from a contaminated parent magma.

Figure 8 examines in more detail the Pb isotopic variations within Sakurajima. At this high resolution, the dacite samples are isotopically indistinguishable from the 1914, 1946 and post 1955 andesites in terms of their overlapping uncertainty ellipses and essentially equivalent average isotope ratios. With the exception of marginally higher ^{208}Pb/^{204}Pb, the Aira caldera rhyolite also has an equivalent isotope composition. There is however an isotopic distinction between these samples and the 4–3.7 ka andesites, particularly apparent in ^{206}Pb/^{204}Pb-^{207}Pb/^{204}Pb (Fig. 8) where there is a clean separation between the uncertainty ellipses of these groups. The 1995 eruption has a more radiogenic signature than the other post 1955 magmatism and the 4–3.7 ka andesites, yet still plots on or within error of the basalt-crust mixing line. The overall elemental composition of the 1995 eruption closely resembles the 1978 and 2000 eruptions, but its Pb isotopes indicate a greater amount of crustal contamination.

It is also noted that the composition of eruptions has become progressively more mafic through the last ~ 500 years, in accordance with the findings of Uto et al. (2005) and

Fig. 8 **a** Average ^{207}Pb/^{204}Pb vs ^{206}Pb/^{204}Pb and **b** average ^{208}Pb/^{204}Pb vs ^{206}Pb/^{204}Pb, for the eruptive products of Sakurajima and Aira caldera. The error ellipses shown are calculated for individual samples. The ellipses are based on the reproducibility of Pb isotope ratios quoted in the "Methods" section. Mixing lines between basalt and Takakumayama granite (pink) and basalt and average Shimanto sediments (black) are shown, along with the basalt-average crust mixing line (brown). Labelled tick marks on this mixing line represent percentage of average crustal melt. Plots **c** and **d** show the basalt-average crust mixing line extrapolated to more radiogenic compositions (dashed brown line). Grey shading highlights compositional field of Shimanto sediments. Data sources as per Fig. 7

- ■ Rhyolite (Aira caldera)
- ◆ Average Dacite
- ✚ Average 4-3.7ka Andesite
- ▲ 1995 eruption
- ■ Average 1914-1946 andesites
- ▲ Average post 1955 andesites
- • Shimanto sediments
- ● Average Shimanto sediments
- ▲ Takakumayama granite
- △ Average crust
- —— Basalt-Average crust mixing line

Takahashi et al. (2013). Figure 3 shows a dacitic composition at ~0.5 ka with 1.5% MgO, through andesites with 2–3% MgO, to the recent eruptions with > 3% MgO. Potentially, this could reflect an increase in the magma throughput in the shallow fractionating reservoir, whereby the more frequent incursion of mafic material progressively weights the overall composition. During this progressive change in major element composition, the Pb isotopes generally are invariant with ^{206}Pb/^{204}Pb ~ 18.40, with the exception of the 1995 eruption with ^{206}Pb/^{204}Pb ~ 18.42 (Fig. 10). This exception suggests that magma supply for individual eruptions can be drawn from a reservoir that has experienced greater crustal contamination.

Elemental-isotopic systematics resulting from assimilation-crystallization in this system are examined in higher resolution in Fig. 9. There appears to be a common fractionation trajectory represented by the samples with ^{206}Pb/^{204}Pb ~ 18.40 that

stems from a ~5% crustal melt addition to the initial basalt. The 4–3.7 ka andesites and 1995 andesite fit with a contribution of ≥6% crust. An alternative explanation to variable quantities of crust in the initial magma is a variation in the proportions of different crustal components. For example, uneven contributions from the upper crustal Shimanto sediments and the lower crustal granites/granodiorites would impart a different Pb isotope signature on the contaminated magma. These magmas could also have assimilated an unknown crustal material of more radiogenic composition, though this cannot be confirmed without better constraining the crustal composition below the volcanic system. Regardless of the contamination systematics, this re-affirms that the supply to individual eruptions, or phases of volcanism, can be sourced from distinct magmas contaminated to different extents. Such distinct magma compositions are only distinguished using this
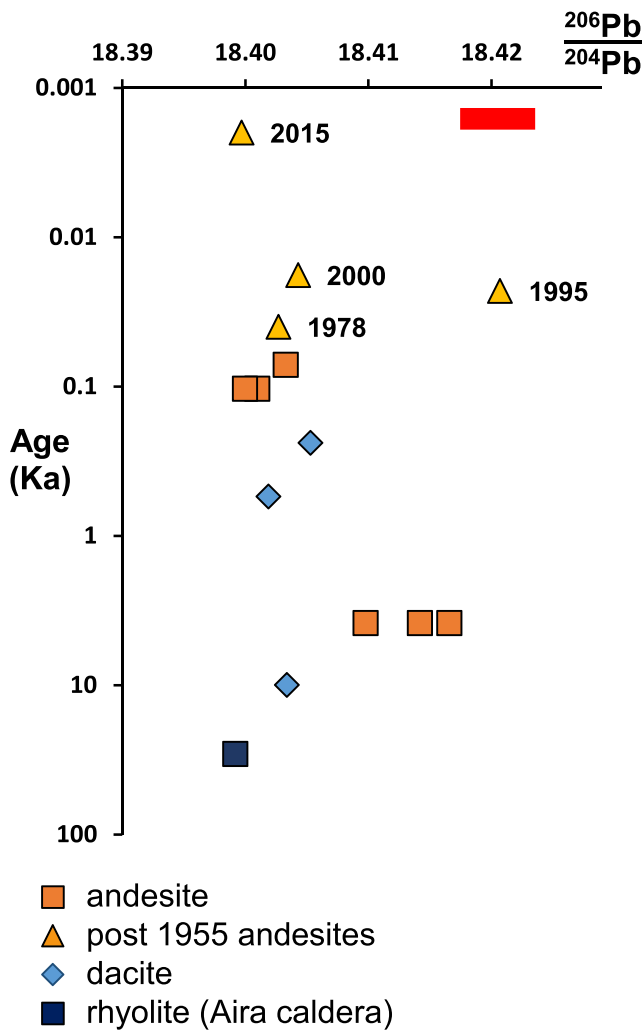
Fig. 9 **a** $^{206}Pb/^{204}Pb$ vs reciprocal concentration of SiO_2 and **b** $^{206}Pb/^{204}Pb$ vs reciprocal concentration of MgO, for the eruptive products of Sakurajima and Aira caldera, basalts and crustal components. Data sources as per Fig. 7. The direction of the black arrow represents an increasing degree of fractional crystallization. Plots **c** and **d** are higher resolution versions of **a** and **b** respectively. The labelled tick marks on the basalt-average crust mixing line represent percentage of average crustal melt. Plots **e** and **f** demonstrate the processes generating the end members of the mixing that produces the magmas erupted in the twentieth century (and possibly earlier eruptions). **e** Contaminated mafic precursory magma undergoes fractional crystallization, producing a silicic magma with the same Pb isotope ratio, stored in the Aira caldera reservoir. **f** Twentieth century: new mafic precursory magma mixes with the silicic magma producing the andesitic magmas of the samples. Mixing end members are the mafic precursory magma, composed of approximately 95% Sumiyoshiike basalt, 5% average crustal melt and silicic/dacitic magma, inferred to have a composition similar to sample YMA 1, the most recently erupted dacite
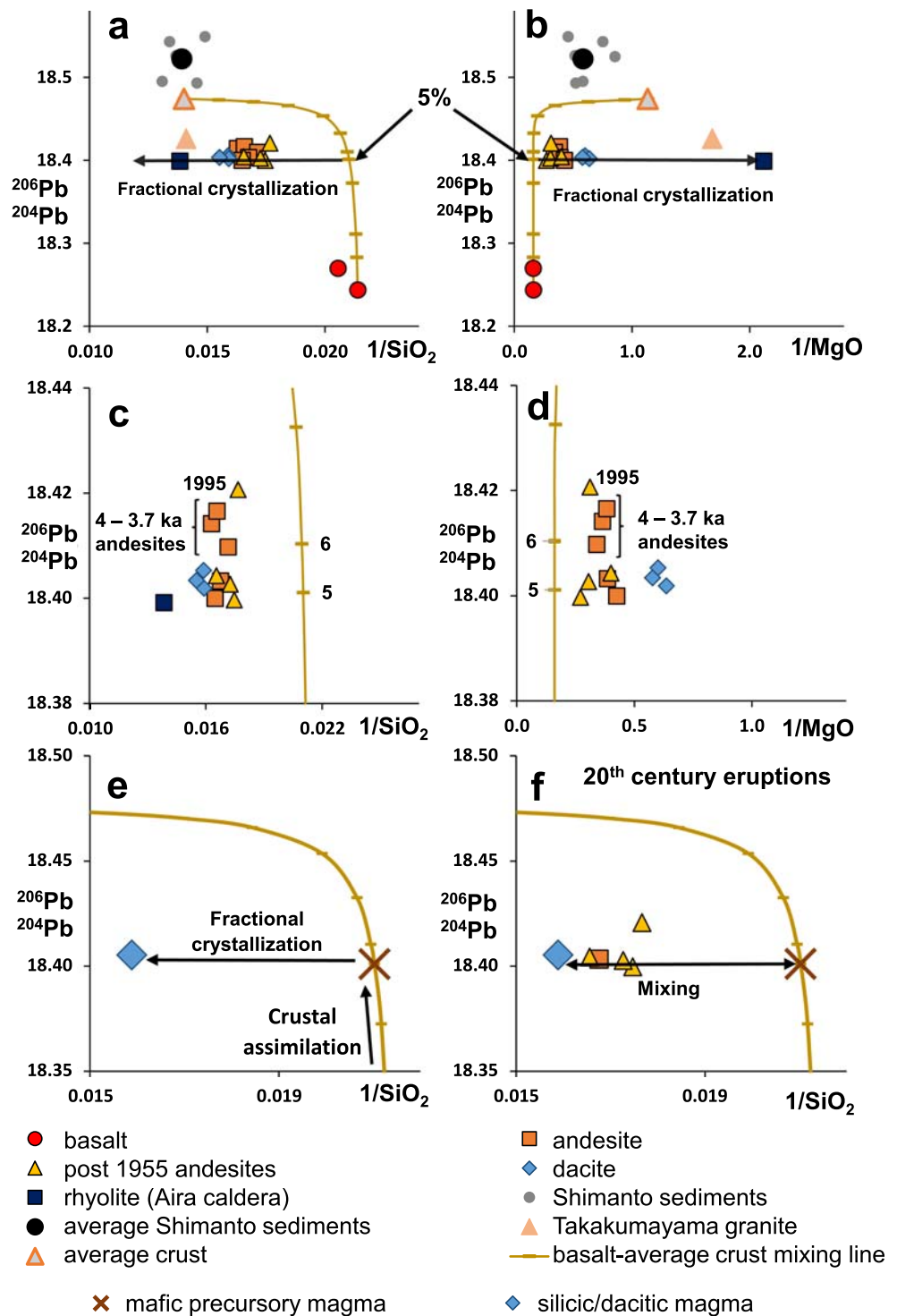
high-precision Pb isotope data and may otherwise go undetected.

Sakurajima incompatible trace element concentrations (e.g. Ba, Rb, La) define a wide range and generally increase with increasing SiO_2, again consistent with fractional crystallization (Appendix D). The lack of correlation between Pb isotopes and incompatible trace element

contents (Appendix D) could be explained by the significant compositional variation in the Shimanto sediments (e.g. 257–689 ppm Ba, 75–232 ppm Rb). This trace element heterogeneity defines a much wider range than the isotopic heterogeneity (Appendix D). Assimilation of sediments with relatively similar isotopic yet highly variable trace element compositions could produce

Fig. 10 Plot of $^{206}Pb/^{204}Pb$ vs age, for the eruptive products of Sakurajima and Aira caldera. The years of post 1955 eruptions are labelled. Red bar indicates uncertainty on $^{206}Pb/^{204}Pb$ measurements

particularly the high $\Delta 7/4$ values of Sakurajima. Hence, a high $\Delta 7/4$-$\Delta 8/4$ component is required in its genesis. An appropriate mantle component would have a Pb isotopic composition similar to the EM2 composition of the Amsterdam Island. However, even this relatively extreme composition ($^{206}Pb/^{204}Pb \sim 19.1$; $\Delta 8/4 \sim 77$) does not have a high enough $\Delta 7/4$ (~ 6) or low enough Ce/Pb (> 15) (Doucet et al. 2004) to act as a suitable component.

The mantle wedge should be the bulk contributor to primitive arc magmas which enter the lithosphere beneath Sakurajima. However, in terms of Pb, the contribution of the MORB-like mantle prior to the addition of fluids from the slab may be reduced or minor (e.g. Straub et al. 2010) given that Ce/Pb is very low in arc magmas (~ 1–8) relative to typical mantle ratios (~ 25). This slab fluid, and the Pb enrichment, originates from the subducting sediments and ocean lithosphere. As such, primitive arc magma is likely to have Pb isotopes that are essentially derived from the melting of a MORB-like mantle that has been hybridized by these slab components (Taylor and Nesbitt 1998).

In the case of Sakurajima, the slab component generating the hybrid mantle is likely to be a PSP sediment-PSP ocean crust mixture (Shinjo et al. 2000). Pb isotope compositional variation within the PSP ocean crust is shown in Fig. 6 and is essentially coincident with Indian MORB. PSP sediments have more radiogenic compositions with $^{206}Pb/^{204}Pb \sim 18.7$ and lower $\Delta 8/4$ relative to Sakurajima. Given these compositions, any fluid-mantle hybridization which integrates PSP sediment, PSP ocean crust and the Indian MORB mantle wedge will not result in the Sakurajima Pb isotope trend.

t could be argued that addition of a more radiogenic subducted sediment with a composition similar to the crustal components used here could explain the isotopic variation without the need for assimilation. PSP sediments have been extensively sampled and measured (Hickey-Vargas 1998; Shimoda et al. 1998), but it is possible that a hitherto unsampled, and isotopically appropriate sedimentary unit exists within the encroaching slab. However, as the regional basaltic lavas are less radiogenic ($^{206}Pb/^{204}Pb \sim 18.25$) than the andesites and dacites ($^{206}Pb/^{204}Pb \sim 18.4$), it is likely that the isotopic variation is generated during crystal fractionation and assimilation in the crust rather than a mantle wedge process.

It is possible that the primary mantle-derived arc magmas may have experienced varying levels of PSP sediment addition. For example, a greater PSP sediment component could give rise to more radiogenic primitive magmas that go on to assimilate crust. In this scenario, the composition of precursory magmas feeding the Sakurajima reservoir would be expected to be more radiogenic, which could offer an alternative explanation to variable levels of crustal addition in producing the higher

isotopically similar mafic precursory magmas with a range of trace element contents that are then further modified by fractional crystallization. Alternatively, the fact that the samples plot on fractionation trend away from the basalt-average crust mixing line on $^{206}Pb/^{204}Pb$ vs incompatible trace element plots (Appendix D) suggests fractional crystallization alone from precursory magmas with consistent trace element compositions could produce the observed variation. Hence, trace elements may not correlate with extent of crustal contamination, as demonstrated by the 4–3.7 ka and 1995 andesites.

A potential cause of Pb isotopic variation at Sakurajima other than crustal contamination is mantle heterogeneity. Although mantle-derived magmas can show considerable compositional variation, as indicated by the Indian and Pacific MORB fields in Fig. 6, isotopic compositions do not reach the high $\Delta 8/4$ and

Fig. 11 Schematic showing the processes involved in the petrogenesis of Sakurajima's magmas. (1) Addition of fluids from the subducting PSP to the mantle wedge causes partial melting. Primitive basaltic magmas form from primary melts. (2) As high-temperature basaltic magma ascends, it induces melting of crustal material. These crustal melts are assimilated by the basaltic magma, in both the lower and upper crusts. (3) Basaltic magma reaches the Aira caldera reservoir with a modified isotopic composition following contamination with crustal melts. This mafic precursory magma then undergoes fractional crystallization, producing silicic magma. More contaminated precursory magmas give rise to more contaminated silicic magmas. Silicic magmas are stored in the Aira caldera reservoir. (4) Injection of mafic magma into stored silicic magmas (and associated mixing) triggers migration from Aira caldera to the shallow Sakurajima reservoir and subsequent eruption. Depths of the brittle-ductile transition and base of the lower crust from Iwasaki et al. (1990) and Kneller et al. (2008), respectively
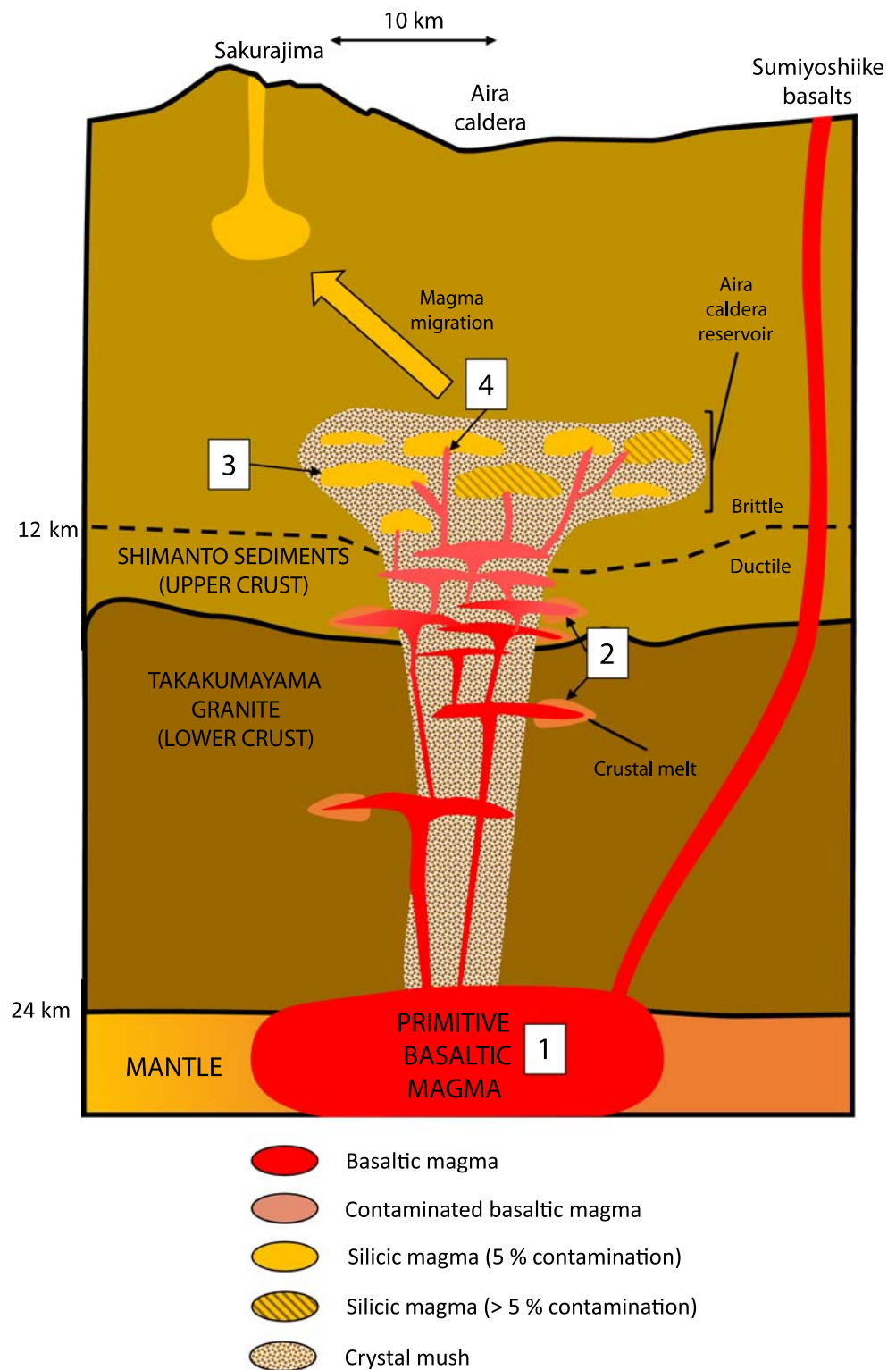
Pb isotope ratios of the 4–3.7 ka andesites and 1995 eruption. Despite this, the proximity of the sample compositions to the basalt-average crust mixing line, and lack of erupted evidence for more radiogenic primitive magmas, suggests that greater crustal contamination is a more realistic explanation.

Eruptive products since 1955

Activity at Sakurajima since 1955 is characterized by frequent Vulcanian explosions (Iguchi 2013). This contrasts with past intermittent larger scale eruptions, suggesting that different processes may be occurring in order to produce this change

in style of activity. Studies of phenocrysts provide evidence for mixing between basaltic and more silicic magmas for the Taisho (1914) and Showa (1946) eruptions (Yanagi et al. 1991; Nakagawa et al. 2011), along with post 1955 eruptions (Nakagawa et al. 2011; Ebihara et al. 2013). This can be reconciled with the Pb isotope data if the basaltic end member of the mixing is taken as the mafic precursory magma that has assimilated crustal materials. Silicic magmas derived from this precursory magma by fractional crystallization would have very similar isotopic ratios to the precursory magma (Fig. 9). The products of mixing of two such magmas would therefore have the same/similar isotopic ratio as the end members, with major element compositions between those of the end members (Fig. 9), lying on an identical trend to that of fractional crystallization. The presence of mafic inclusions in the An-ei dacites suggests that injection and mixing of basaltic magma into more silicic magma also occurred in 1779 (Yanagi et al. 1991). Such studies have not examined older eruptions; hence, the extent to which these involved mixing cannot be constrained.

The lower SiO_2 and higher MgO of the post 1955 andesites indicate a greater basaltic contribution to the final erupted mixed magma relative to the 1914 and 1946 eruptions. This can only be determined from major and trace element data and is not distinguishable isotopically, since the post 1955 mafic end member appears to be contaminated with crust to the same extent as precursory magmas feeding older eruptions. However, the isotopic data does identify that, in the case of the 1995 eruption, at least one of the mixing end member magmas was more crustally contaminated. The incompatible trace element concentrations (e.g. Ba, Rb, Pb) of this sample are lower than other post 1955 eruptions, closer to the basalts. This suggests that this eruption likely involved a significant mafic component (possibly one less enriched in incompatible trace elements than Sumiyoshiike basalt), reducing incompatible trace element and silica content, mixed with a more contaminated silicic magma (derived from an older, more contaminated mafic precursory magma), producing the more radiogenic isotopic composition.

The only discernible change in petrogenetic processes since 1955 is an increased mafic component in erupted mixed magmas, likely due to increased throughput of mafic magma to the Aira caldera reservoir. This supports the conclusions of Nakagawa et al. (2011), who suggest that recent Vulcanian eruptions at Sakurajima are triggered by frequent injection of basaltic magma, which has caused the change in style of activity. Crustal contamination processes prior to crystallization and/or mixing in the Aira caldera reservoir appear to have remained consistent across the post 1955 transition. Individual eruptions and phases of activity involving more radiogenic magmas have occurred both pre and post 1955, suggesting that differences in extent of crustal contamination are not linked to the change in style of activity.

Petrogenetic model for Sakurajima volcano

Figure 11 shows a schematic model for the petrogenesis of Sakurajima-Aira magmas, based on the findings detailed above combined with geophysical observations. Seismic data has demonstrated the existence of a shallow magma reservoir below Sakurajima (3–6 km depth) and deeper magma reservoir below Aira caldera (approximately 10 km depth) (Iguchi 2013). Primitive basaltic magma assimilates both lower and upper crustal materials, prior to reaching the Aira caldera magma reservoir. Hence, crustal assimilation occurs at depths greater than 10 km in the magma plumbing system. The contaminated mafic precursory magma then undergoes fractional crystallization, producing silicic magmas that are stored in the reservoir. Variation in the extent to which precursory magma is contaminated gives rise to silicic magmas of variable Pb isotope compositions (Fig. 11). Fresh injection of mafic magma into stored silicic magmas likely triggers eruptions (Nakagawa et al. 2011; Ebihara et al. 2013). Studies of vertical ground deformation and observed migration of A-type earthquake hypocentres to shallower depths provide evidence for magma migration to the shallow reservoir below Sakurajima during eruptive episodes (Iguchi 2013). Increased mafic magma throughput since 1955 has resulted in eruption of mixed magmas with an increasing basaltic component, producing the recent trend towards lower silica eruptive products.

The Aira caldera rhyolite, dacites erupted at 10 ka, 1471 and 1779, and post 1914 eruptive products all share a similarly contaminated precursor magma and/or mixing end members. More contaminated magmas were involved in the petrogenesis of the andesites erupted between 4 and 3.7 ka and in 1995.

Conclusions

This study uses high-resolution Pb isotopes to assess crustal assimilation and temporal changes in magma petrogenesis in the Sakurajima-Aira volcanic system. The Sakurajima-Aira caldera volcano has significantly more radiogenic Pb isotopes and higher $\Delta 7/4Pb$ and $\Delta 8/4Pb$ than local basaltic eruptions. This can be attributed to assimilation of lower and upper crustal materials, represented in terms of Pb isotope compositions by the locally exposed Takakumayama granite and Shimanto sediments respectively, by these primitive basaltic magmas. Assimilation occurs prior to differentiation and mixing processes at depths greater than 10 km.

The Pb isotope ratios of the Sakurajima-Aira system eruptive products show little variation with increasing SiO_2 and decreasing MgO content, suggesting they are derived from fractional crystallization of a similarly

contaminated precursor magma. This precursor is consistent with addition of 5–6% average crustal melt to a primitive basaltic magma. When the high-resolution Pb isotopes are examined in detail, it is recognized that andesites erupted between 4–3.7 ka and the 1995 eruption contain a greater proportion of crustal contamination. This suggests that distinct magma compositions were available to feed particular eruptions or eruptive phases. Only from such high-precision data can these variations in the extent of crustal contamination be detected. This demonstrates the value of high-resolution Pb isotope analysis in assessing short-term changes in magma-crust interaction.

Final erupted magmas post 1955, along with those from 1914 and 1946 (and possibly older eruptions), were produced by mixing of basaltic (contaminated precursory magma) and stored silicic magmas with essentially identical isotopic ratios. Andesitic pyroclastics erupted since 1955 typically have lower SiO_2 and higher MgO than older lava flows, but (mostly) display equivalent Pb isotope ratios. This can be attributed to a greater throughput of contaminated mafic magma to the Aira caldera reservoir since 1955, resulting in eruption of mixed magmas with a greater mafic component. The extent of crustal contamination before and after 1955 has remained consistent; hence, it is unlikely to be a contributing factor to the transition in activity style.

Application of high-resolution Pb isotopes to other arc volcanoes may reveal subtle variations in the magmas feeding eruptions that previously went undetected by elemental and lower resolution isotopic analyses. Combining this technique with major element and phenocryst data as in this study also provides a tool with which to explore whether there exists a relationship between crustal contamination and surface activity in volcanic systems.

Compliance with ethical standards

Conflict of interest   The authors declare that they have no competing interests.

References

Abouchami W, Galer S, Hofmann A (2000) High precision lead isotope systematics of lavas from the Hawaiian Scientific Drilling Project. Chem Geol 169:187–209

Aramaki S (1984) Formation of the Aira Caldera, southern Kyushu, ~22,000 years ago. J Geophys Res 89(B10):8485

Armstrong R (1971) Isotopic and chemical constraints on models of magma genesis in volcanic arcs. Earth Planet Sci Lett 12:137–142

Asmerom Y, Jacobsen S (1993) The Pb isotopic evolution of the Earth: inferences from river water suspended loads. Earth Planet Sci Lett 115:245–256

Cassidy M, Taylor R, Palmer M, Cooper R, Stenlake C, Trofimovs J (2012) Tracking the magmatic evolution of island arc volcanism: insights from a high-precision Pb isotope record of Montserrat, Lesser Antilles. Geochem Geophys Geosyst 13:5

Croudace I, Williams-Thorpe O (1988) A low dilution, wavelength dispersive X-ray fluorescence procedure for the analysis of archaeological rock artefacts. Archaeometry 30:227–236

Davidson J, Hora J, Garrison J, Dungan M (2005) Crustal forensics in arc magmas. J Volcanol Geotherm Res 140:157–170

Doucet S, Weis D, Scoates J, Debaille V, Giret A (2004) Geochemical and Hf–Pb–Sr–Nd isotopic constraints on the origin of the Amsterdam–St. Paul (Indian Ocean) hotspot basalts. Earth Planet Sci Lett 218:179–195

Ducea M, Saleeby J, Bergantz G (2015) The architecture, chemistry, and evolution of continental magmatic arcs. Annu Rev Earth Planet Sci 43:299–331

Dupré B, Allègre C (1983) Pb–Sr isotope variation in Indian Ocean basalts and mixing phenomena. Nature 303:142–146

Ebihara K, Nakagawa M, Matsumoto A, Amma-Miyasaka M and Iguchi M (2013) Evolution of magma plumbing system of Sakurajima Volcano in the last 50 years: frequent vulcanian eruptions controlled by basalt injection. IAVCEI 2013 Scientific Assembly Kagoshima 183

Elburg M, Foden J (1998) Temporal changes in arc magma geochemistry, northern Sulawesi, Indonesia. Earth Planet Sci Lett 163:381–398

Elliott T (2004) Tracers of the slab. In: Eiler J (ed) Inside the subduction factory. American Geophysical Union, Washington, pp 23–45

Fukuyama H (1978) Geology of Sakurajima volcano, southern Kyushu. J Geol Soc Japan 84:309–316

Gómez-Tuena A, LaGatta A, Langmuir C, Goldstein S, Ortega-Gutiérrez F, Carrasco-Núñez G (2003) Temporal control of subduction magmatism in the eastern Trans-Mexican Volcanic Belt: mantle sources, slab contributions, and crustal contamination. Geochem Geophys Geosyst 4:8

Grove T, Kinzler R, Baker M, Donnelly-Nolan J, Lesher C (1988) Assimilation of granite by basaltic magma at Burnt Lava flow, Medicine Lake volcano, northern California: decoupling of heat and mass transfer. Contrib Mineral Petrol 99:320–343

Hanyu T, Tatsumi Y, Nakai S, Chang Q, Miyazaki T, Sato K, Tani K, Shibata T, Yoshida T (2006) Contribution of slab melting and slab dehydration to magmatism in the Japanese arc. Geochim Cosmochim Acta 70:229

Harmon R, Barreiro B, Moorbath S, Hoefs J, Francis P, Thorpe R, Déruelle B, McHugh J, Viglino J (1984) Regional O-, Sr-, and Pb-isotope relationships in late Cenozoic calc-alkaline lavas of the Andean Cordillera. J Geol Soc 141:803–822

Hart S (1984) A large-scale isotope anomaly in the Southern Hemisphere mantle. Nature 309:753–757

Hawkesworth C, Gallagher K, Hergt J, McDermott F (1993) Mantle and Slab Contributions in Arc Magmas. Annual Review of Earth and Planetary Sciences 21:175-204

Hickey-Vargas R (1998) Origin of the Indian Ocean-type isotopic signature in basalts from Philippine Sea plate spreading centers: an

assessment of local versus large-scale processes. J Geophys Res Solid Earth 103(B9):20963–20979

Hildreth W, Moorbath S (1988) Crustal contributions to arc magmatism in the Andes of Central Chile. Contrib Mineral Petrol 98:455–489

Hosono T, Nakano T (2003) Petrochemistry of volcanic rocks in the Hishikari mining area of southern Japan, with implications for the relative contribution of lower crust and mantle-derived basalt. Resour Geol 53:239–259

Hosono T, Nakano T, Murakami H (2003) Sr–Nd–Pb isotopic compositions of volcanic rocks around the Hishikari gold deposit, southwest Japan: implications for the contribution of a felsic lower crust. Chem Geol 201:19–36

Hosono T, Nakano T, Shin K, Murakami H (2008) Assimilation of lower to middle crust by high alumina basalt magma as an explanation for the origin of medium-K volcanic rocks in southern Kyushu, Japan. Lithos 105:51–62

Iguchi M (2013) Magma movement from the deep to shallow Sakurajima volcano as revealed by geophysical observations. Bull Volcanol Soc Japan 58:1–18

Ishihara S, Chappell B (2010) Chemical compositions of the Miocene granitoids of the Okueyama, Hoei mine and Takakumayama plutons, Outer Zone of SW Japan. Bull Geol Surv Jpn 61:17–38

Ishizuka O, Yuasa M, Taylor R, Sakamoto I (2009) Two contrasting magmatic types coexist after the cessation of back-arc spreading. Chem Geol 266:274–296

Ishizuka O, Yuasa M, Tamura Y, Shukuno H, Stern R, Naka J, Joshima M, Taylor R (2010) Migrating shoshonitic magmatism tracks Izu–Bonin–Mariana intra-oceanic arc rift propagation. Earth Planet Sci Lett 294:111–122

Ishizuka O, Taylor R, Geshi N, Oikawa T, Kawanabe Y, Ogitsu I (2015) Progressive mixed-magma recharging of Izu-Oshima volcano, Japan: a guide to magma chamber volume. Earth Planet Sci Lett 430:19–29

Ishizuka O, Taylor R, Geshi N, Mochizuki N (2017) Large-volume lateral magma transport from the Mull volcano: an insight to magma chamber processes. Geochem Geophys Geosyst 18:1618–1640

Iwasaki T, Hirata N, Kanazawa T, Melles J, Suyehiro K, Urabe T, Möller L, Makris J, Shimamura H (1990) Crustal and upper mantle structure in the Ryukyu Island Arc deduced from deep seismic sounding. Geophys J Int 102:631–651

Jochum KP, Nohl U, Herwig K, Lammel E, Stoll B, Hofmann AW (2005) GeoReM: a new geochemical database for reference materials and isotopic standards. Geostand Geoanal Res 29:333–338

Kayzar T, Nelson B, Bachmann O, Bauer A and Izbekov P (2014) Deciphering petrogenic processes using Pb isotope ratios from time-series samples at Bezymianny and Klyuchevskoy volcanoes, Central Kamchatka Depression Contributions to Mineralogy and Petrology 168

Kneller E, Long M, van Keken P (2008) Olivine fabric transitions and shear wave anisotropy in the Ryukyu subduction system. Earth Planet Sci Lett 268:268–282

Kobayashi T, Miki D, Sasaki H, Iguchi M, Yamamoto T and Uto K (2013) Geological map of Sakurajima volcano. Geological Maps of Volcanoes, 1

Kuritani T, Kitigawa H, Nakamura E (2005) Assimilation and fractional crystallization controlled by transport process of crustal melt: implications from an alkali basalt–dacite suite from Rishiri volcano, Japan. J Petrol 46(7):1421–1442

Labanieh S, Chauvel C, Germa A, Quidelleur X, Lewin E (2010) Isotopic hyperbolas constrain sources and processes under the Lesser Antilles arc. Earth Planet Sci Lett 298:35–46

Matsui T (2006) Partial replacement of plagioclase by smectite within the Takakumayama granite, Kagoshima, Japan. J Mineral Petrol Sci 101:329–333

Matsumoto A, Nakagawa M, Amma-Miyasaka M and Iguchi M (2013) Petrological monitoring of volcanic ash and evaluation of on-going eruptive activity of Sakurajima volcano, Japan: characterization of juvenile magma and its evolution since 2006. IAVCEI 2013 Scientific Assembly Kagoshima 639

Meyzen C, Blichert-Toft J, Ludden J, Humler E, Mével C, Albarède F (2007) Isotopic portrayal of the Earth's upper mantle flow field. Nature 447:1069–1074

Miki D (1999) Estimate of the ages of lava flows at Sakurajima volcano, Kyushu, Japan; inferred from paleomagnetic directions and paleointensities. Bull Volcanol Soc Japan 44:111–122

Nakagawa M, Matsumoto A, Amma-Miyasaka M and Iguchi M (2011) Change of mode of eruptive activity and the magma plumbing system of Sakurajima volcano since 20th century. Japan Geoscience Union Meeting 2011

Plank T, Langmuir C (1998) The chemical composition of subducting sediment and its consequences for the crust and mantle. Chem Geol 145:325–394

Pouclet A, Lee J, Vidal P, Cousens B, Bellon H (1994) Cretaceous to Cenozoic volcanism in South Korea and in the Sea of Japan: magmatic constraints on the opening of the back-arc basin. Geol Soc London Spec Publ 81:169–191

Shibata T, Suzuki J, Yoshikawa M, Kobayashi T, Miki D, Takemura K (2013a) Geochemical and Sr-Nd-Pb isotopic constraints on the origin and magmatic evolution of Quaternary lavas of Sakurajima volcano, southern Kyushu Island, Japan. Bull Volcanol Soc Japan 58:43–58

Shibata T, Yoshikawa M, Itoh J, Ujike O, Miyoshi M, Takemura K (2013b) Along arc geochemical variations in Quaternary magmas of northern Kyushu Island, Japan. Geol Soc London Spec Publ 385:15–29

Shimoda G, Tatsumi Y, Nohda S, Ishizaka K, Jahn B (1998) Setouchi high-Mg andesites revisited: geochemical evidence for melting of subducting sediments. Earth Planet Sci Lett 160:479–492

Shin K (2008) Geochemical study of the back arc Tsushima granite pluton and its comparison to the other Middle Miocene granites in southwest Japan. PhD thesis, University of Tsukuba

Shinjo R, Woodhead J, Hergt J (2000) Geochemical variation within the northern Ryukyu Arc: magma source compositions and geodynamic implications. Contrib Mineral Petrol 140:263–282

Straub S, Goldstein S, Class C, Schmidt A, Gomez-Tuena A (2010) Slab and mantle controls on the Sr–Nd–Pb–Hf isotope evolution of the post 42 Ma Izu–Bonin volcanic arc. J Petrol 51:993–1026

Straub S, Woodhead J, Arculus R (2015) Temporal evolution of the Mariana Arc: mantle wedge and subducted slab controls revealed with a tephra perspective. J Petrol 56:409–439

Sun SS, McDonough WS (1989) Chemical and isotopic systematics of oceanic basalts: implications for mantle composition and processes. Geol Soc London Spec Publ 42:313–345

Takahashi M, Otsuka T, Sako H, Kawamata H, Yasui M, Kanamaru T, Otsuki M, Kobayashi T, Ishihara K, Miki D (2013) Temporal variation for magmatic chemistry of the Sakurajima volcano and Aira caldera region, southern Kyushu, Southwest Japan since 61ka and its implications for the evolution of magma chamber system. Bull Volcanol Soc Japan 58:19–42

Taylor S, MacLennan S (1985) The continental crust: its composition and evolution. Blackwell, Oxford

Taylor R, Nesbitt R (1998) Isotopic characteristics of subduction fluids in an intra-oceanic setting, Izu–Bonin Arc, Japan. Earth Planet Sci Lett 164:79–98

Taylor R, Ishizuka O, Michalik A, Milton J, Croudace I (2015) Evaluating the precision of Pb isotope measurement by mass spectrometry. J Anal At Spectrom 30:198–213

Uto K, Miki D, Nguyen H, Sudo M, Fukushima D, Ishihara K (2005) Temporal evolution of magma composition in Sakurajima volcano, southwest Japan. Ann Disaster Prev Res Inst Kyoto Univ 48B:341–347

Workman R, Hart S (2005) Major and trace element composition of the depleted MORB mantle (DMM). Earth Planet Sci Lett 231:53–72

Yanagi T, Ichimaru Y, Hirahara S (1991) Petrochemical evidence for coupled magma chambers beneath the Sakurajima volcano, Kyushu, Japan. Geochem J 25:17